The EMBO Journal (2004) 23, 1536–1546 | © 2004 European Molecular Biology Organization | All Rights Reserved 0261-4189/04
www.embojournal.org

THE EMBO JOURNAL

Dynacortin contributes to cortical viscoelasticity and helps define the shape changes of cytokinesis

Kristine D Girard[1], Charles Chaney[2], Michael Delannoy[1], Scot C Kuo[2] and Douglas N Robinson[1,*]

[1]Department of Cell Biology, Johns Hopkins University School of Medicine, Baltimore, MD, USA and [2]Department of Biomedical Engineering, Johns Hopkins University School of Medicine, Baltimore, MD, USA

During cytokinesis, global and equatorial pathways deform the cell cortex in a stereotypical manner, which leads to daughter cell separation. Equatorial forces are largely generated by myosin-II and the actin crosslinker, cortexillin-I. In contrast, global mechanics are determined by the cortical cytoskeleton, including the actin crosslinker, dynacortin. We used direct morphometric characterization and laser-tracking microrheology to quantify cortical mechanical properties of wild-type and *cortexillin-I* and *dynacortin* mutant *Dictyostelium* cells. Both cortexillin-I and dynacortin influence cytokinesis and interphase cortical viscoelasticity as predicted from genetics and biochemical data using purified dynacortin proteins. Our studies suggest that the regulation of cytokinesis ultimately requires modulation of proteins that control the cortical mechanical properties that establish the force-balance that specifies the shapes of cytokinesis. The combination of genetic, biochemical, and biophysical observations suggests that the cell's cortical mechanical properties control how the cortex is remodeled during cytokinesis.

The EMBO Journal (2004) **23,** 1536–1546. doi:10.1038/sj.emboj.7600167; Published online 11 March 2004
Subject Categories: cell & tissue architecture; cell cycle
Keywords: cell morphology; cortical mechanics; cytokinesis; *Dictyostelium*; rheology

Introduction

Cytokinesis is the mechanical process that cleaves a mother cell into two daughter cells and is essential for the propagation of cells across all phylogeny (Robinson and Spudich, 2000b). After more than 100 years of study, the fundamental mechanical bases for metazoan cytokinesis are still not understood, let alone the molecular bases for these mechanical elements (Rappaport, 1996). Two predominant models have been debated in recent decades: equatorial stimulation and polar relaxation (White and Borisy, 1983; Devore *et al*, 1989). The equatorial stimulation model assigns active force production to the contractile ring, which is considered a myosin-II-driven process (Robinson *et al*, 2002b). In contrast, the polar relaxation model assigns the polar cortex as the major source of active force production. As the volume of the mother cell is conserved during division, expansion of the polar cortex leads to cleavage furrow ingression. The role of myosin-II in the polar relaxation model is to serve as a dynamic actin crosslinker, increasing the equatorial stiffness so that the cleavage furrow ingresses.

Still, recent studies have been unable to clarify the mechanical mechanisms of cytokinesis. Myosin-II is required for cytokinesis in suspension culture, while adherent mitotic ameboid *myosin-II* mutant cells divide nearly normally (DeLozanne and Spudich, 1987; Knecht and Loomis, 1987). Pharmacological inhibition of the polar cortex with actin filament destabilizers inhibits furrow ingression, whereas introduction of the inhibitors in the furrow region accelerated ingression of the cleavage furrow (O'Connell *et al*, 2001). By atomic force microscopy, which measures the bending modulus perpendicular to the cell's surface, the mammalian cell equator was more stiff than the basal global stiffness of the cell, a property that is most likely ubiquitous among metazoan-like cytokineses (Matzke *et al*, 2001). These results suggest that the global and equatorial cortices have distinct and important roles in cytokinesis.

Force-balance is a principle fundamental to all mechanical shape changes. We have proposed a force-balance hypothesis in which the amount of contractile force generated by the contractile ring is specified by the mechanical resistance provided by the global cortex. A significant component of our hypothesis is that different mechanical elements are generated by specific proteins and that genetic interactions between these proteins reveal how they modulate different mechanical elements (Robinson and Spudich, 2000a; Robinson, 2001; Robinson *et al*, 2002b). In the force-balance hypothesis, at least three idealized mechanical elements are involved in cell shape changes. These elements include an active equatorial constricting force, cortical stretch modulus, and cytoplasmic viscosity. The active constricting forces for cytokinesis are proposed to be produced largely by equatorially localized myosin-II (Robinson and Spudich, 2000b). The cortical stretch modulus is the energy cost for deforming the cell. The stretch modulus is generated by cortical actin filaments and crosslinkers, and has been shown to be a strong predictor of how much myosin-II is recruited to the cleavage furrow cortex (Robinson *et al*, 2002a). As actin crosslinkers are dynamic, the cell's cortex is neither purely viscous nor elastic but has both viscous and elastic characteristics (Sato *et al*, 1987; Wachsstock *et al*, 1993, 1994; Xu *et al*, 1998). Cytoplasmic viscosity is the energy cost for bulk flow and the ratio of the stretch modulus to the cytoplasmic viscosity is predicted to set the rate of furrow ingression (Zhang and Robinson, in preparation).

Genetic studies using *Dictyostelium discoideum* have identified proteins that are predicted to influence cortical viscoelasticity during cytokinesis (Robinson and Spudich, 2000a;

*Corresponding author. Department of Cell Biology, Johns Hopkins University School of Medicine, 725 North Wolfe Street, Baltimore, MD 21205-2196, USA. Tel.: + 410 502 2850;
E-mail: dnr@jhmi.edu

Received: 5 December 2003; accepted: 19 February 2004; published online: 11 March 2004

Weber *et al*, 2000). Efficient cytokinesis requires different actin filament crosslinking proteins with different cellular distributions (Robinson and Spudich, 2000a). Dynacortin is an actin filament bundling protein that was originally identified in a genetic selection for suppressors of mutants devoid of cortexillin-I, an actin crosslinking protein (Faix *et al*, 1996, 2001; Robinson and Spudich, 2000a). The suppression experiment was performed with a cDNA expression library and only the carboxyl-half (C181) of dynacortin suppressed *cortexillin-I* (Robinson and Spudich, 2000a). In contrast, overexpression of the full-length dynacortin not only failed to rescue *cortexillin-I* but it also induced a dominant cytokinesis defect (Robinson and Spudich, 2000a). Dynacortin is distributed around the cell cortex, while cortexillin-I is concentrated in the equatorial cortex (Weber *et al*, 1999; Robinson and Spudich, 2000a). The cellular distributions and the genetic interactions of cortexillin-I and dynacortin suggest that they cooperate with each other to modulate the cortical mechanics that drive the complex shape changes of cytokinesis.

In this paper, we combine biochemistry, genetics, direct observation of cytokinesis, and cellular biophysics to dissect the function of dynacortin and the basis for its genetic interactions with cortexillin-I. A significant new technical development is our ability to quantify the mechanical impact that dynacortin and cortexillin-I have on cell cortices, using a new noninvasive technology, laser-tracking microrheology (LTM) (Gittes *et al*, 1997; Mason *et al*, 1997; McGrath *et al*, 2000; Yamada *et al*, 2000). Several observations emerge from this study. First, we report the first loss-of-function phenotype for dynacortin, assigning a role for dynacortin, like cortexillin-I, in modulating the cortical viscoelasticity of interphase cells and specifying the shapes of cytokinesis. Second, dynacortin has two independent actin crosslinking domains, amino-half (N173) and C181, that crosslink with different relative activities. Third, our data suggest that the activities of proteins that are predicted to have different kinetics of actin crosslinking may be distinguished *in vivo* using LTM. Finally and most significantly, this study provides essential groundwork for determining how global and equatorial actin crosslinking specifies the shapes and ultimately the dynamics of cytokinesis.

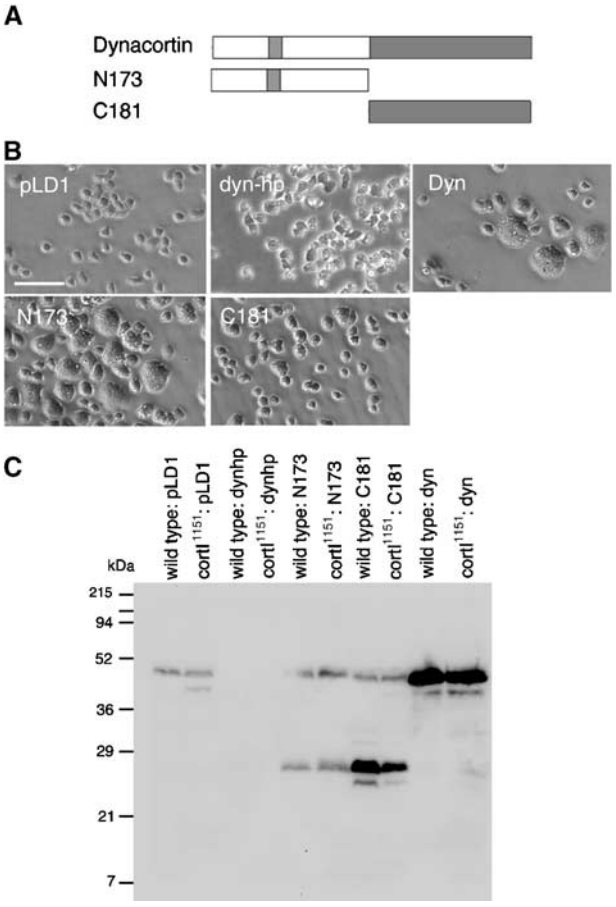

Figure 1 (**A**) The cartoon represents the dynacortin proteins studied. (**B**) Micrographs of wild-type (wt:pLD1) cells carrying the control plasmid pLD1A15SN or an expression plasmid for dynacortin hairpin (dynhp), full-length dynacortin (Dyn), N173, or C181; scale bar, 40 μm. (**C**) Western immunoblot using antidynacortin polyclonal antibodies of cells expressing various *dynacortin* constructs. pLD1 is the expression vector used to express each protein in *Dictyostelium* and control strains were transformed with the empty vector.

Results

Dynacortin and cortexillin-I have quantitative effects on cell growth

To initiate this study, we characterized the growth effects of a *dynacortin* hairpin construct (dynhp) that silenced *dynacortin* expression. The expression of dynhp led to a complete loss of detectable dynacortin and resulted in mild changes in the rate of increase of cell number as compared to wild type and *cortexillin-I* controls (Figure 1C; Table I). We examined the cell size and relative growth rates of cells expressing each of the dynacortin domains for direct comparison to dynhp (Figure 1B and C; Table I). By microscopy, full-length dynacortin induced a 'big-cell' phenotype in wild type (Figure 1B) and *cortexillin-I* (data not shown), as observed previously (Robinson and Spudich, 2000a). Interestingly, N173 also induced a similar phenotype. C181 cells were uniform in size and rescued the growth rate as shown previously (Figure 1B, Table I; Robinson and Spudich, 2000a).

To compare directly the *in vivo* morphological, growth, and mechanical effects (below) with the affinities and activities measured *in vitro*, we quantified the expression levels of each dynacortin domain in wild-type and *cortexillin-I* mutant strains (see Materials and methods). The cellular concentrations are presented (Table I). Although some of the protein concentrations appear unusually high, in fact the cellular concentrations of each domain are consistent with the biochemical activities of each protein (below; compare Table I with Table II).

Dynacortin, N173, and C181 crosslink actin but with different activities

To elucidate dynacortin's molecular mechanisms, we analyzed dynacortin, C181, and N173 for their hydrodynamic properties and interactions with actin filaments (Table II, Supplementary Results and Supplementary Figures 1–3). Hydrodynamically, dynacortin is a rod-shaped dimer and the core of dimerization resides in the C181 domain (Supplementary Figure 1, Supplementary Table 1). Both N173 and C181 bind and crosslink actin *in vitro* with similar

Table I Quantification of cellular growth rates and cellular concentrations of dynacortin and its domains

Strain	Relative growth rate[a] (*n*)	% Total protein (*n*)	[monomer], μM	[dimer][b], μM
Wild type: pLD1A15SN	[100%] (12)	0.03% (4)	2	1
cortI^{1151}: pLD1A15SN	54% (12)	0.03% (4)	2	1
Wild type: dynhp	110% (6)	0.0% (8)	—	—
cortI^{1151}: dynhp	40% (6)	0.0% (8)	—	—
Wild type: N173	96% (8)	0.4% (2)	50	NA
cortI^{1151}: N173	21% (6)	0.4% (4)	50	NA
Wild type: C181	88% (14)	0.5% (4)	60	30
cortI^{1151}: C181	80% (10)	0.5% (2)	60	30
Wild type: dynacortin	61% (8)	0.3% (3)	20	10
cortI^{1151}: dynacortin	35% (8)	0.2% (3)	10	5

[a]Relative growth rates were measured as the increase in cell number in suspension culture. All strains were normalized to wild type: pLD1A15SN controls, which is bracketed to indicate that fact.
[b]Dynacortin and C181 form dimers while N173 exists as monomers (Supplementary Figure 1; Supplementary Table 1).

Table II Summary of actin-binding parameters for dynacortin, N173, and C181

Protein	K_{D1app}, μM (*n*)	K_{D2app}, μM (*n*)	$(K_{D1app})^2K_{D2app}$, μM^3	Half-maximal concentrations[a]	
				Fluorescence assay	Falling ball viscometry
Dynacortin	8.7±1.3 (6)	1.3±0.2 (17)	98	0.5 μM	0.5–1 μM
N173	9.4±1.3 (10)	6.1±0.9 (21)	540	60 μM	50–60 μM
C181	19±2.9 (7)	2.0±0.4 (20)	720	8 μM	15 μM

K_{D1app} increased with increasing actin concentration. This is likely due to actin polymers getting buried in the actin bundle so that it was more difficult for dynacortins to saturate each available site. The listed K_{D1app} data are based on 5-μM actin-binding isotherms. Data from first binding step fit a model of a single binding isotherm, and the same saturation stoichiometry was observed at every actin concentration. For the 5-μM actin data, the χ^2 values obtained by comparing the data to a simulated square hyperbola using the measured K_{D1app} value ranged from 0.05 to 0.1 ($P>0.20$). Thus, the model is not rejected and K_{D1} appears to be only [actin]-dependent, not [crosslinker]-dependent. K_{D2app} is based on all data as this parameter did not appear to be [actin]-dependent over greater than an order of magnitude of actin concentrations. Both K_D values are only apparent values as dynacortin proteins that are bound and forming crosslinks versus those that are only bound cannot be cleanly separated by cosedimentation analysis.
[a]Concentrations are for dimeric dynacortin and C181 and monomeric N173.

apparent thermodynamics, but with different overall activities as determined by falling ball viscometry and quantitative fluorescence microscopy (Table II; Supplementary Figures 2, 3). Using actin cosedimentation, falling ball viscometry, and the fluorescence microscopy assay, we determined an activity order for actin crosslinking as: Dynacortin > C181 > N173 (Table II). The half-maximal concentrations for bundle formation determined from the fluorescence assay and falling ball viscometry are in good agreement with the actual amounts of each protein expressed in cells (Compare Tables I and II). As N173 and C181 had similar thermodynamics but C181 appeared to be a more effective crosslinker than N173, we hypothesize that N173 may have faster on and off rates to achieve the same actin crosslinking equilibrium.

Dynacortin and cortexillin-I have complementary distributions during cytokinesis; C181 and N173 are distributed between the cytoplasm and cortex

We examined the subcellular localization of dynacortin, N173, and C181 in interphase and dividing cells. Each protein was detected in two ways: GFP-fusions (GFP-dynacortin, GFP-N173 or C181-GFP) were imaged in live interphase cells (Figure 2A), and untagged proteins were imaged by immunocytochemistry in fixed dividing cells (Figure 2B). Both types of detection gave similar results for the localization of each protein. Only GFP-dynacortin and overexpressed untagged dynacortin showed clear enrichment in the cortex (Figure 2A and B). Cells expressing *dynacortin*-hairpin (dynhp), which had >99% reduction in the dynacortin level, had only a low level of background fluorescence when examined by immunocytochemistry (Figure 2B). Endogenous dynacortin is distributed between the cytoplasm and cortex in dividing cells (Figure 2B). Overexpressed full-length dynacortin showed a clear cortical enrichment in dividing cells (Figure 2B). N173 showed some cortical localization by both methods (Figure 2A and B), while C181 appeared to be distributed evenly between the cortex and cytoplasm (Figure 2A and B). To compare the localization of dynacortin to cortexillin-I, we examined the distribution of a GFP-tagged cortexillin-I expressed in a *cortexillin-I* mutant cell line (*cortI^{1151}*:GFP-cort; Figure 2C). Cortexillin-I localized to the contractile ring in agreement with previously published observations (Weber *et al*, 1999).

Dynacortin and cortexillin-I control the morphology of cytokinesis

To ascertain dynacortin's and cortexillin-I's role in cytokinesis, we examined the morphology of dividing cells (Figure 3).

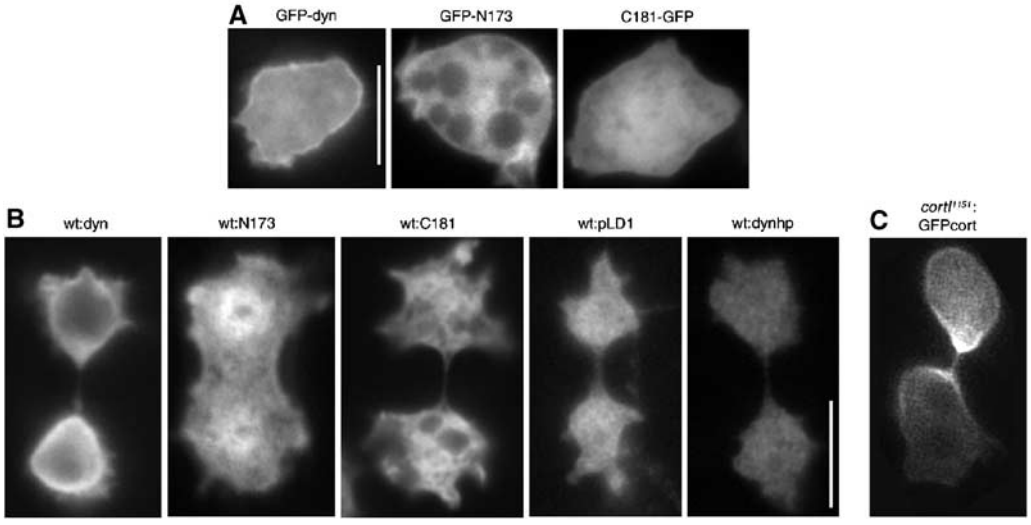

Figure 2 Dynacortin, N173, and C181 are globally distributed during cytokinesis. (**A**) GFP-dynacortin, GFP-N173, and C181-GFP were examined in live wild-type interphase cells; scale bar, 10 μm. (**B**) Total dynacortin was imaged by immunocytochemistry of dividing wild-type cells carrying episomal expression plasmids using antidynacortin polyclonal antibodies. Endogenous dynacortin (wt:pLD1) and wild-type cells expressing dynacortin-hairpin (wt:dynhp), which reduced dynacortin expression by >99%, are also presented. As the N173 and C181 domains are overexpressed, the pattern that is revealed is largely due to the transgene product. (**C**) A *cortexillin-I* mutant cell complemented with a GFP-cortexillin-I construct (*cortI*^{1151}:GFPcort) is shown to indicate the distribution of cortexillin-I during cytokinesis. Scale bar (10 μm) in B applies to B and C.

We monitored the velocity of furrow ingression, whether the cleavage furrow ingressed evenly from both sides and whether the daughter cells were equal in size (Table III). To monitor the kinetics of furrow ingression, we measured the time-dependent change of the furrow diameter and the length of the furrow, which ultimately formed a bridge before being severed (Figure 3A). Wild-type cells always formed a discrete bridge relatively early in the process, and the bridge length always started smaller than the furrow diameter (Figure 3B). As the furrow continued to constrict, at some point the cylindrical bridge length and diameter were equal to each other. The distance when the furrow length and diameter were equal is defined as the crossover distance (D_x). Subsequently, the bridge became longer than the diameter as the furrow diameter continued to decrease before being severed.

Deletion of *cortexillin-I* or silencing of *dynacortin* altered the morphology of cytokinesis (Figure 3C and D; Table III). Silencing of *dynacortin* caused the cells to appear more rounded during division and led to a large decrease in the crossover distance (Figure 3C; Table III). Deletion of *cortexillin-I* reduced the efficiency of cytokinesis, leading to a higher rate of failures, unequal cleavage events, and asymmetric ingression of the furrow (Table III). We focused on successful divisions so that the morphology (crossover distance and symmetry of furrow ingression) and velocities of furrow ingression could be fully assessed. Therefore, our data likely under-represent the unequal cleavage rate and cytokinesis failure rate as compared to other studies of *cortexillin-I* mutants (Weber *et al*, 2000). The crossover distance and symmetry of the cleavage furrows of *cortexillin-I* mutants were rescued by cortexillin-I (Table III) and dynacortin C181 (Figure 3E; Table III). Thus, even though dynacortin C181 and cortexillin-I have different cellular distributions during cytokinesis (Figure 2), both proteins quantitatively rescue the morphology of dividing *cortexillin-I* mutant cells.

Laser-tracking microrheology allows quantitative analysis of cortical mechanics

To quantify the effects of dynacortin and cortexillin-I on cortical mechanics, we used laser-tracking microrheology (LTM) to measure cortical viscoelasticity of wild-type and mutant cell lines (Figure 4; Mason *et al*, 1997; McGrath *et al*, 2000; Yamada *et al*, 2000). With LTM, the viscoelasticity of materials may be measured across a frequency spectrum by monitoring the motions of a spherical bead immersed in the material. Typically, viscoelastic moduli are measured when all dimensions of the material are nearly infinite relative to the bead. As cell cortices are sheet-like and often much thinner than the particles, we chose to measure the frequency-dependent viscoelasticity, $|\mu^*|$, which is a phenomenological spring constant with viscous damping (see Methods for equations and rationale).

To determine cortical viscoelasticity, the thermal motions of a bead on a cell were monitored (at 6 kHz) for eleven 1-s intervals and then the viscoelasticity was calculated as the average of these 11 sequential measurements. For windows of time greater than 1 s, the bead's motions were often obscured by the cell's motion. Therefore, we restricted our observations to timescales shorter than 1 s. For physiological relevance, we focused on the longer timescales from 500-ms timescale (2 rad/s) to 5-ms timescale (200 rad/s).

To verify that LTM of beads placed on the cell's extracellular surface would report on the underlying cytoskeleton, we compared wild-type cells to wild-type cells treated with latrunculin B, a potent F-actin depolymerizing agent (Figure 5A and B). In all, 85% of the viscoelasticity of wild-type cells was lost upon treatment with latrunculin B. As latrunculin B treatment results in depolymerization of filamentous actin, the 15% of viscoelasticity that remains presumably is due to the lipid bilayer and underlying cytosol.

LTM also permits measurement of the phase angle, a property that reflects the solid-like or liquid-like nature of

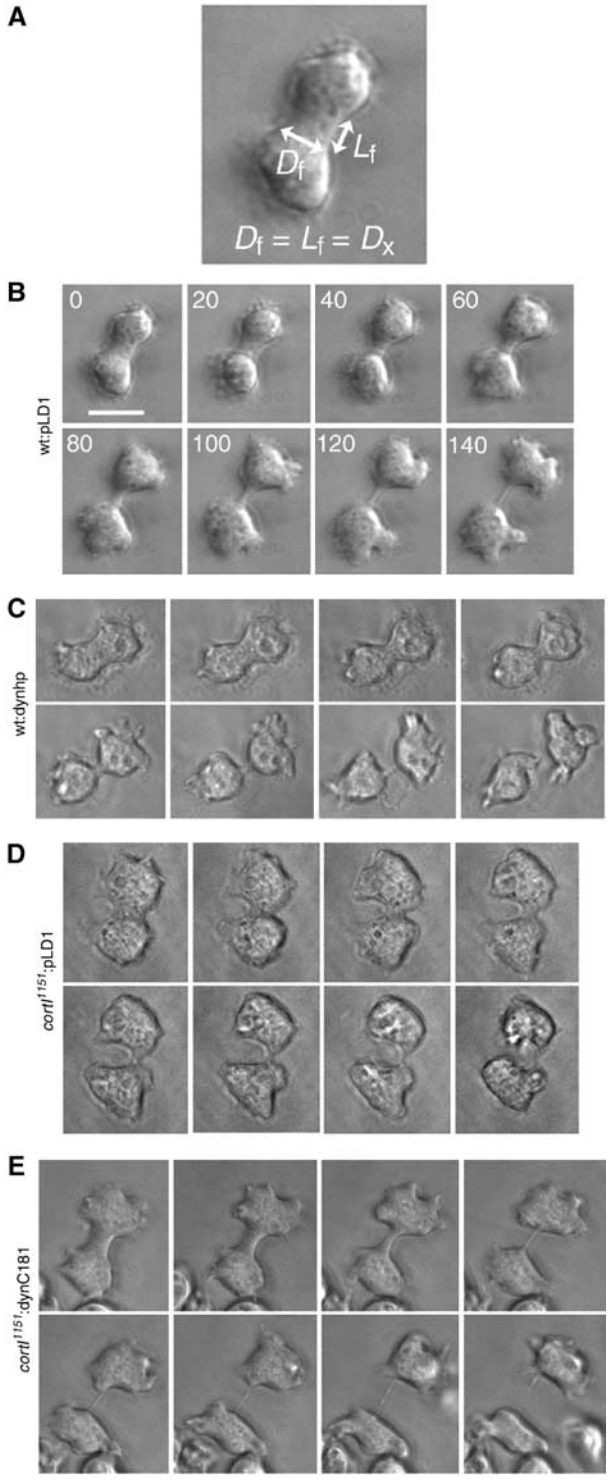

Figure 3 Analysis of the morphology of cytokinesis of wt:pLD1, wt:dynhp, *cortI*^{1151}:pLD1 and *cortI*^{1151}:C181 cells. (**A**) Diagram depicts the furrow diameter (D_f) and the furrow length (L_f), which were measured to determine the crossover distance, D_x. D_x is defined as the distance where D_f equals L_f. (**B**) Wt:pLD1 cells form a distinct bridge relatively early during the process. (**C**) Wt:dynhp cells form a distinct bridge at a later stage and appear more rounded in general. (**D**) This *cortI*^{1151}:pLD1 cell formed a bridge at a later stage and the furrow ingression was faster on one side than the other. (**E**) The morphology of the *cortexillin-I* mutant cytokinesis was rescued by dynacortin C181. The furrow ingressed symmetrically and a distinct bridge was formed at an earlier stage similar to wild type; scale bar, 10 μm.

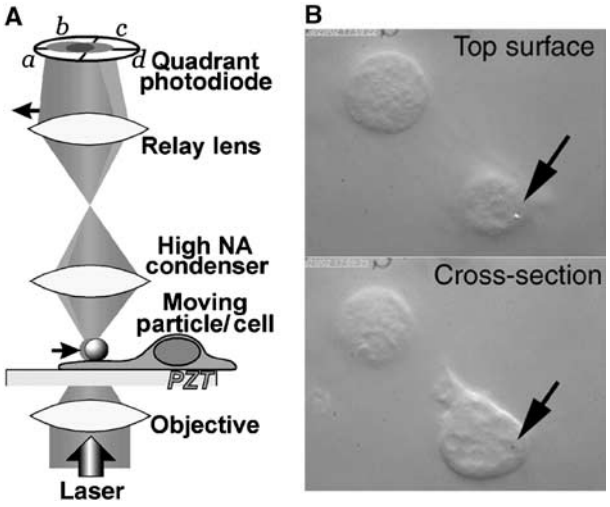

Figure 4 Laser-tracking microrheology (LTM) system for measuring cortical mechanics. (**A**) The LTM system utilizes a low-power laser that is focused by the objective on a 0.7 μm polystyrene bead resting on the surface of the cell. As thermal energy drives the motion of the bead, the laser beam is deflected. The deflections are relayed via a condenser and relay lens to a quadrant photodiode detector, which monitors bead position. (**B**) Upper panel: To measure the cortical mechanical properties, a negatively charged polystyrene bead (arrow) is allowed to settle onto the surface of the cell, attaching nonspecifically. By focusing on the top surface of the cell, the bead is visible. Lower panel: By focusing on a lower cross-section, pseudopods can be seen. An arrow marks the *XY*-position of the bead.

a material. As the material becomes more solid-like, the phase angle tends towards 0 and as the material becomes more liquid-like, the phase angle tends towards 90°. Pure actin networks and Cos7 lamellae have a characteristic phase angle of 22° (at 10 rad/s; Yamada *et al*, 2000). We extracted the phase angle data for each strain to determine how liquid- or solid-like the respective strains are. The average phase angles for all *Dictyostelium* strains ranged between 15 and 22°, which is similar to the phase angle of pure actin. In fact, none of the strains showed a difference greater than 2° across the full frequency range. In contrast, latrunculin B generally increased the phase angle (to around 30°) particularly at higher frequencies, indicating that the cell cortex was partially liquefied by the depolymerization of the actin filaments. Therefore, even though the beads are on the extracellular surface of the plasma membrane, the bead reports on a mechanical environment that is largely dependent on the cortical actin cytoskeleton and that has material properties (phase angle) similar to pure actin.

Loss of dynacortin or cortexillin-I reduces cortical viscoelasticity

By LTM analysis, removal of dynacortin and/or cortexillin-I had quantitative effects on cortical viscoelasticity (Figures 5 and 6; Supplementary Table 2). Deletion of *cortexillin-I* reduced the cortical viscoelasticity by approximately 30% across the full frequency spectrum as compared to the wild-type strain (Figure 5C, panel 1; 5D). The distribution of viscoelastic values of *dynacortin* silenced cells was much more heterogeneous with many more high-end outliers than wild-type parental cells were; therefore, we present histograms of viscoelastic measurements at two frequencies for

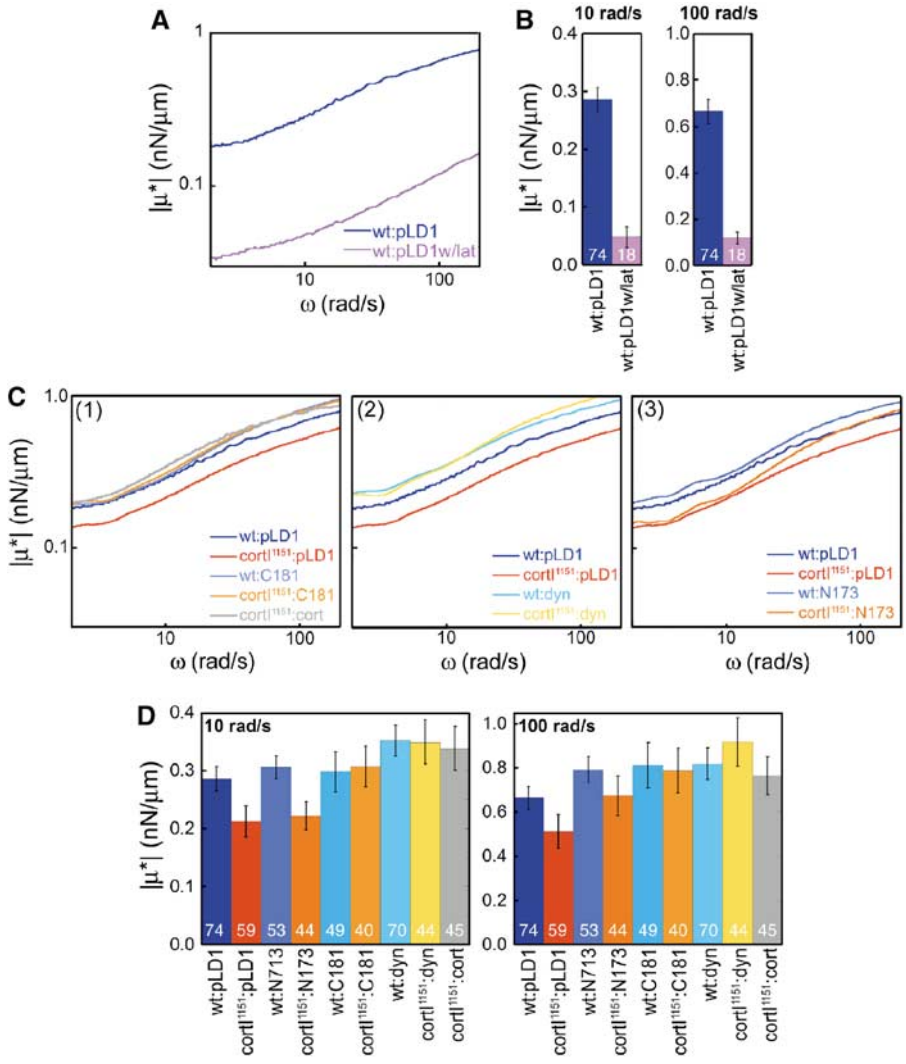

Figure 5 Dynacortin and its domains alter cortical viscoelasticity. (**A**) Frequency spectra of wild-type cells (wt:pLD1) and wt:pLD1 treated with latrunculin B show that actin filaments are necessary for 85% of cortical viscoelasticity. (**B**) Histograms of wt:pLD1 versus wt:pLD1 treated with latrunculin B at 10 and 100 rad/s for statistical comparison. *n* values are shown on bars. *P*-values from Student's *t*-test are <0.0001 at both frequencies. (**C**) Frequency spectra of viscoelasticity of wild-type and cortexillin-I mutant cells expressing dynacortin full-length, N173, C181, and cortexillin-I proteins. All spectra are the average spectra for each strain. The numbers of cells measured for each genetic strain are shown on the histrogram in part D. All measurements were made on 'wild-type'-sized cells to prevent possible complications due to cell size differences. The wild-type control spectrum is shown in each panel for direct comparison. (**D**) Histograms of means ($\pm$s.e.m.) for the viscoelasticity at 10 and 100 rad/s. These values correspond to the frequency spectra in (A). *n* values for each strain are listed on the bars in the histograms. For significance, the *P*-values from pairwise Student's *t*-test are presented in Supplemental Table 2.

wild-type and *cortexillin-I* mutant cells with and without dynacortin (Figure 6). Silencing of *dynacortin* in wild-type cells resulted in a 50% reduction in the median cortical viscoelasticity (Figure 6, panels 1, 2 versus 3, 4). Interestingly, the *cortexillin-I* background (Figure 6, panels 5, 6 versus 7, 8) seemed to be more resistant to the loss of dynacortin than the wild-type cells were. For example, silencing of *dynacortin* in wild-type cells reduced viscoelasticity from 0.28 to 0.14 nN/μm (at 10 rad/s), while in the *cortexillin-I* background, the numbers remained similar (0.17 versus 0.20 nN/μm at 10 rad/s). This resistance might reflect the antagonistic role proposed for these two proteins in promoting cytokinesis (Robinson and Spudich, 2000a). Alternatively, the *cortexillin-I* mutant cells may have adapted to the absence of cortexillin-I and the same safeguards protect the cell from the loss of dynacortin. Nevertheless, dynacortin and cortexillin-I modulate cortical mechanics and both may help keep the cortex relatively uniform in its mechanical properties.

Overexpressing dynacortin, C181 and N173 reveal additional important cortical mechanical properties

We used LTM to examine the effects of C181 and cortexillin-I on the *cortexillin-I* mutant's cortical viscoelasticity (Figure 5C, panel 1; 5D). We found that C181 rescued cortical viscoelasticity to wild-type levels across all frequencies examined, while cortexillin-I actually restored the viscoelasticity to slightly above wild-type levels. The rescue of *cortexillin-I* mutant's cortical mechanics by cortexillin-I and C181 correlates well with their rescue of *cortexillin-I* mutant cells' cytokinesis morphology and ability to grow in suspension culture.

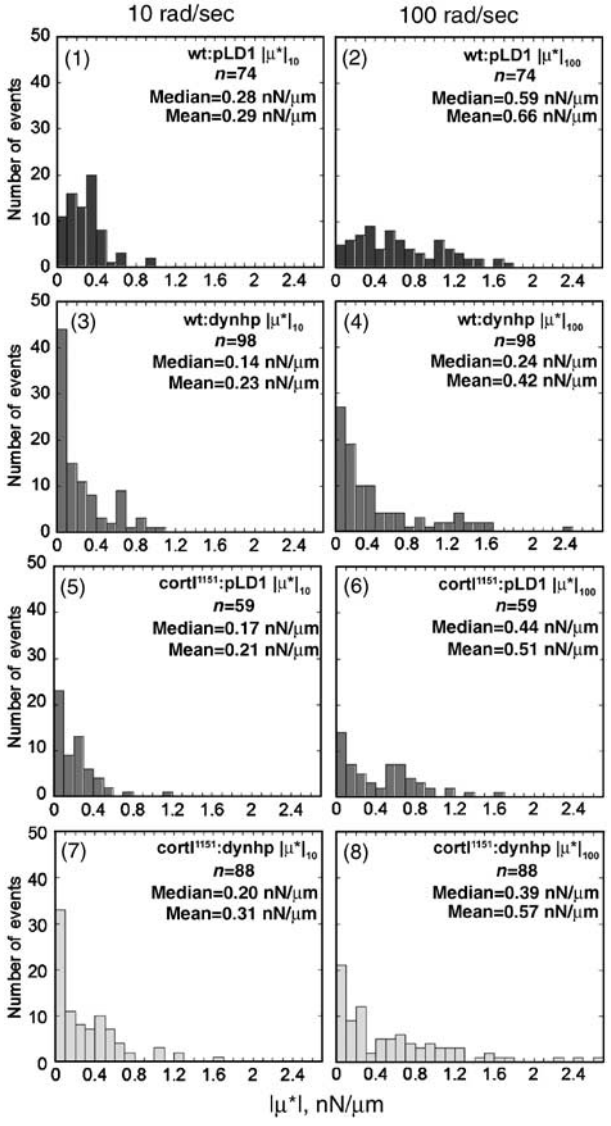

Figure 6 Dynacortin is required for normal cortical viscoelasticity. Silencing of *dynacortin* reduced the median cortical viscoelasticity and led to greater skewing of the frequency distribution, which is indicative of greater heterogeneity of the viscoelasticity of the cortex. As the mean is very sensitive to skewing and heterogeneity while the median is more resistant, the medians for each strain are emphasized. The means are presented for comparison. The frequency distribution of viscoelastic measurements from wild-type cells (wt:pLD1) at 10 rad/s was monomodal but was more broadly distributed at 100 rad/s. The wt:pLD1 medians were very similar to the means indicating monodispersity and therefore, greater homogeneity of the wild-type cortex. Wt:dynhp cells devoid of dynacortin showed a skewed distribution with increased heterogeneity at both frequencies. *Cortexillin-I* mutants (*cortI*^{1151}:pLD1) were intermediate between wt:pLD1 and wt:dynhp cells at both frequencies. The *cortI*^{1151}:dynhp (*dynacortin/cortexillin-I* double mutant) cells were similar to *cortI*^{1151}:pLD1 cells. As wt:dynhp, *cortI*^{1151}:pLD1, and *cortI*^{1151}:dynhp distributions were skewed, we compared the distributions to wt:pLD1 using a one-tailed, nonparametric Mann–Whitney–Wilcoxson *U*-test, which makes no assumptions about the shape of the distributions. $|\mu^*|_{10}$ and $|\mu^*|_{100}$ values for wt:dynhp ($P<0.001$) and *cortI*^{1151}:pLD1 ($P<0.005$) were significantly less than wt:pLD1. The distributions of $|\mu^*|_{10}$ and $|\mu^*|_{100}$ values for *cortI*^{1151}:dynhp were also smaller than the distributions of values for wt:pLD1 ($|\mu^*|_{10}$; $P=0.11$ and $|\mu^*|_{100}$; $P=0.01$).

We also analyzed the cortical mechanics of dynacortin and N173 overexpressing cells (Figure 5C, panels 2 and 3; 5D). Previously, we showed that dynacortin overexpressers are variable in size, probably due to a defect in the efficiency of cytokinesis rather than a complete loss of cytokinesis. To avoid possible mechanical changes due to size differences rather than differences in dynacortin-mediated actin crosslinking, we restricted our LTM measurements to the subpopulation of cells that were similar in size to wild-type cells. Overexpression of dynacortin increased cortical viscoelasticity to levels higher than wild type across the full range of frequencies examined, regardless of the genetic background, wild type or *cortexillin-I* (Figure 5C, panel 2; 5D). By contrast, N173 rescued the cortical viscoelasticity of the *cortexillin-I* mutant cells only at high frequencies (above 40 rad/s); at lower frequencies, *cortexillin-I* cells expressing N173 showed only a small increase in cortical viscoelasticity (Figure 5C, panel 3; 5D). N173's behavior of increasing cortical viscoelasticity at higher frequencies is consistent with a crosslinking protein that has faster kinetics. Indeed, our biochemical analysis of N173 has suggested that it crosslinks actin with faster kinetics than either full-length dynacortin or C181 do. Thus, our current data suggest that LTM can discriminate between different crosslinking kinetic properties *in vivo*.

It is notable that N173, C181, and dynacortin have larger relative effects in a *cortexillin-I* background than they do in a wild-type background. In fact, the *cortexillin-I* background is necessary for observing the frequency-dependent behavior of N173. However, the actual $|\mu^*|$ values achieved by each respective overexpressed dynacortin protein are similar in both genetic backgrounds. As the expression levels in each background are similar, the biochemical components that generate cellular mechanical properties may be saturable (Figure 5, Table I).

Discussion

In this paper, we present the first characterization of the loss-of-function phenotype of dynacortin, including its role in cytokinesis, characterize dynacortin's actin crosslinking mechanisms, and demonstrate that dynacortin and cortexillin-I control the viscoelastic properties of the cell cortex. We examine several aspects of the morphology of cytokinesis of mutant strains with altered dynacortin and/or cortexillin-I function and introduce a novel metric, D_x. This analysis reveals that dynacortin and cortexillin-I specify the dimensions and morphology of the cleavage furrow. Furthermore, from our biochemical analyses of dynacortin and actin interactions *in vitro*, we demonstrate that the specific molecular interactions quantitatively specify both morphology and mechanics.

LTM, a powerful technique for measuring cortical mechanics

We used LTM to measure the cortical viscoelasticity of wild-type and *cortexillin-I* mutant cells expressing dynacortin, N173, C181, or cortexillin-I. Quantitatively, our measurements by LTM agree with measurements from other techniques. Our LTM measurement of wild-type cortical viscoelasticity was 0.3 nN/μm (at 10 rad/s), which is in reasonable agreement with the cortical stretch modulus (1.5 nN/μm) measured by microcapillary aspiration

Table III Average velocity of furrow ingression and crossover distance for each strain

Strain	Velocity[a] (μm/*s*) (*n*)	Cross-over length, D_x[b] (μm) (*n*)	Symmetric daughters[c]/symmetric furrows[d] (*n*)
Wild type: pLD1	0.029±0.0032 (21)	2.7±0.16 (21)	100%/100% (24)
Wild type: dynhp	0.033±0.0023 (14)	1.5±0.20 (14)	88%/100% (17)
cortI^{1151}: pLD1	0.032±0.0030 (16)	2.2±0.19 (16)	80% (30)/50% (22)
cortI^{1151}: cortI	0.027±0.0027 (6)	2.5±0.068 (6)	100%/100% (6)
cortI^{1151}: C181	0.037±0.0026 (19)	3.0±0.14 (19)	100%/95% (19)

[a]The velocity is the average velocity of furrow ingression.
[b]Crossover length is an objective morpho-metric parameter in which the length of cleavage furrow bridge is equal to the diameter of the cleavage furrow. The crossover length serves to distinguish quantitatively morphologies between different strains. Values are mean±s.e.m. Wild type:pLD1, *cortI*^{1151}: C181 and *cortI*^{1151}:cortI are all statistically indistinguishable. Wild type: dynhp ($P<0.00005$) and *cortI*^{1151}: pLD1 ($P<0.05$) are significantly less than the wild-type control. *cortI*^{1151}: C181 is significantly greater than *cortI*^{1151}: pLD1 ($0.0005<P<0.005$).
[c]The cells were assessed qualitatively as to whether the daughter cells were symmetric in size.
[d]The furrows were assessed for being symmetrically positioned and whether they ingressed similarly from both sides.

(Gerald *et al*, 1998; Dai *et al*, 1999). Considering that the scale of the deformations from each technique differs by an order of magnitude, the agreement between values from the two techniques is remarkable. In principle, the cortical viscoelasticity measured by LTM and the cortical stretch modulus measured by microcapillary aspiration are similar parameters. However, LTM has the important advantage of generating time-dependent information that reflects the kinetics of actin crosslinking.

Across greater than two decades of mechanical frequency, silencing of *dynacortin* caused a severe reduction (50%) in cortical viscoelasticity, while deletion of *cortexillin-I* caused a significant reduction (30%) in cortical viscoelasticity. For *cortexillin-I*, the reduction we measured with LTM matches the reduction previously reported using nontime-resolved methods (Simson *et al*, 1998). Genetically rescuing *cortexillin-I* with either cortexillin-I or C181 restored cortical viscoelasticity to wild-type levels. In contrast, overexpressing dynacortin elevated the viscoelasticity of both wild-type and *cortexillin-I* mutant cells across all frequencies, possibly explaining the dominant cytokinesis defect induced by this construct. From our *in vitro* studies, we predicted that N173 would have differential effects, depending on the mechanical frequencies, because of its predicted faster binding kinetics. Indeed, N173 increased the viscoelasticity of wild-type and *cortexillin-I* mutant cells only slightly at a low mechanical frequency but restored the cortical viscoelasticity of *cortexillin-I* mutant cells to wild-type levels at higher frequencies. Thus, cortical mechanics are controlled biochemically, can be dissected genetically, and can be measured using LTM.

Crossover distance as a critical cytokinesis metric

The shapes of cytokinesis are very stereotypical and include a final bridge stage in which the bridge, connecting the two daughter cells, is cylindrical in shape. This regularity allows the bridge to be analyzed using means typical of highly quantitative studies of fluid breakup of viscoelastic fluids (Entov and Hinch, 1997; Zhang and Lister, 1999). The regularity is nicely reflected in the crossover distance, D_x, which appears to be a fingerprint for each genetic strain (Table III). Previously, we hypothesized that the amount of force required of the contractile ring may be related to the stretch modulus of the cortex; indeed, this relationship accurately predicts the myosin-II amounts sent to the contractile ring (Robinson *et al*, 2002a). In this working hypothesis (Figure 7), the size of the vectors reflects this balance. In our working model, we propose that D_x might reflect the

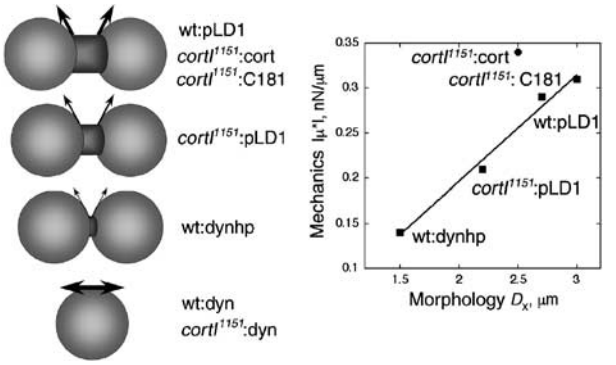

Figure 7 A hypothesis for how cortical mechanics might specify the shapes of cytokinesis. The morphology is schematized, and the arrows represent the restoring vectors that are hypothesized to counteract the contractile force. To summarize the data presented in this paper, we present a graph, comparing D_x measured by direct observation of cytokinesis and |μ*| from the interphase mechanical measurements from LTM. The line is a linear fit (correlation coefficient of 0.99) to all points except the *cortI*^{1151}:cort (see Discussion).

magnitude of the restoring vector that counteracts the pulling force that the contractile ring exerts on the cell's cortex. We speculate that D_x is a balancing point where the forces of the contractile ring balance the largely elastic properties of the rest of the cortex. Higher values of viscoelasticity mean that the cortex deforms less in response to a force. Hence, the contractile ring does not constrict as much by the time D_x is reached. In contrast, if cells are softer, then the contractile ring advances further yielding a smaller D_x. After the balancing point defined by D_x, cells appear to enter a new phase where furrow thinning follows a different kinetic behavior (Zhang and Robinson, in preparation).

To summarize the data from this paper into a framework, we present a plot of the measured D_x and |μ*| values, which were correlated (Figure 7). Each of the 'wild-type-like' strains has a larger D_x and |μ*| than the loss-of-function *cortexillin-I* or *dynacortin* hairpin mutants. Cells overexpressing dynacortin have greater viscoelasticity. The viscoelasticity increase might be responsible for the dominant cytokinesis defect observed in these cells by making it more difficult for the contractile ring to contract. Due to the low frequency of division events in the dynacortin overexpressing strains, D_x has not yet been quantified. Interestingly, the *cortI*^{1151}:cort cells' |μ*| versus D_x point falls somewhat off of the line, possibly as cortexillin-I enriches in the cleavage furrow cortex

but is not excluded from the global cortex. Further, expression of cortexillin-I in a *cortexillin-I* mutant (*cortI*^{1151}:cort) elevates cortical viscoelasticity to above wild-type levels probably because expression from an episomal plasmid is not as well controlled as the endogenous locus. Thus, if cortexillin-I specifically increases the viscoelasticity of the cleavage furrow cortex to above wild-type levels, the furrow cortex may stretch less as it constricts, resulting in a slightly smaller D_x.

The interpretation of the correlation in Figure 7 currently remains a hypothesis, as viscoelastic measurements used interphase, rather than mitotic, cells. Currently, technical issues prevent us from measuring viscoelasticity of mitotic cells using LTM. Specifically, to get the beads to adhere to the cell surface, the cells must be plated in starvation buffer. This condition significantly reduces the frequency of cytokinesis events. In other work, we have quantified the dynamics of cleavage furrow ingression of wild-type, *myosin-II*, *RacE*, *dynacortin*, and *cortexillin-I* mutant strains (Zhang and Robinson, in preparation). By comparing the kinetics of furrow thinning to fluid mechanical models, we determined the function of each protein during cytokinesis. Further, from the cytokinesis dynamics analysis, we calculated cortical stretch modulus values that closely match the viscoelasticity values measured by LTM. Ultimately, the mitotic values for viscoelasticity may prove to be related to interphase values as the global cortex of dividing mammalian cells became uniformly four-fold more stiff than interphase levels (measured with atomic force microscopy, AFM) (Matzke *et al*, 2001). In the AFM study, the equatorial region continued to rise in stiffness beyond this four-fold increase, perhaps due to the activity of proteins providing a similar function as cortexillin-I does in *Dictyostelium*. If *Dictyostelium* cells are similar to mammalian cells, the correlation in Figure 7 may simply shift up (perhaps four-fold as in mammalian cells) to account for the different cell cycle stage.

C181 compensation for cortexillin-I

Previously, we showed that dynacortin C181 rescued the growth rate and gross cytokinesis defect of *cortexillin-I* (Robinson and Spudich, 2000a). Here, we demonstrate that C181 rescues the cleavage furrow morphology, including shape and dimensions, and the interphase cortical viscoelasticity of *cortexillin-I* mutant cells. With the mechanical and biochemical data in hand, three mechanisms might explain how C181 compensates for cortexillin-I. As cortexillin-I and myosin-II are not exclusively concentrated in the contractile ring, both proteins may contribute to global mechanical properties as well as equatorial contractility (reviewed in Robinson *et al*, 2002b). Dynacortin C181 might rescue cortexillin-I's role in global viscoelasticity, indicating a level of functional redundancy. Second, C181 may have an indirect effect on the contractile ring by stiffening the global cortex, thereby refocusing the equatorial contractility of *cortexillin-I* mutant cells. As C181 is reduced in the furrow region, the cleavage furrow cortex and cytoplasm may have lower viscoelasticity so that this region is more deformable, allowing the *cortexillin-I* mutant contractile ring to constrict through a softer region of the cell. A similar phenomenon has been observed in mammalian cells when disruption of the equatorial cytoskeleton by pharmacological inhibition accelerated the rate of cleavage furrow ingression (O'Connell *et al*, 2001). In addition, a third mechanism is suggested from the combination of our LTM, biochemical, and dynamics data (this paper; Zhang and Robinson, in preparation). In this hypothesis, global actin crosslinking mediated by dynacortin (and C181) and equatorial actin crosslinking mediated by cortexillin-I have distinct roles in governing the fluid dynamics of furrow ingression.

Cortical mechanics and dynamics of furrow ingression

Our mechanical measurements may also help explain the kinetics of shape changes. Quantitatively, the stretch modulus and cytoplasmic viscosity should combine to regulate the speed of cleavage furrow shape changes for a given force. As an initial model, the ratio of cortical stretch modulus to viscosity should determine the velocity of shape changes (such that $v = S_c/3\mu$ where v is the velocity, S_c is the stretch modulus, and μ is the viscosity) (Entov and Hinch, 1997). Using 0.3 nN/μm (wild type at 10 rad/s; this paper) or 1.5 nN/μm for S_c (Gerald *et al*, 1998; Dai *et al*, 1999) and the largest measured cytoplasmic viscosity (0.35 nN s/μm^2; Feneberg *et al*, 2001), velocities in the 1–2 μm/s range are predicted. For furrow ingression, these velocities are 50-fold faster than observed for wild-type cells (Table III). However, bridge retraction (after the intercellular bridge is severed) velocities are on the 1–2 μm/s range and agree with these predictions (Zhang and Robinson, in preparation). Thus, the dynamics of bridge retraction can be described in terms of fluid mechanical properties. In contrast, we have identified *Dictyostelium* mutants where cleavage furrow ingression achieves velocities predicted from the pure fluid mechanical considerations (Zhang and Robinson, in preparation).

As it is the energy cost for deforming the cell, the cortical stretch modulus has two opposing roles that are separated temporally during cytokinesis. As the mother cell and two daughter cells are nearly spherical, these shapes may be thought of as equilibrium states. As the mother cell begins to elongate and form the furrow, it reaches a transition state that is an energy barrier between two equilibrium states. Therefore, the larger the stretch modulus, the larger the energy barrier. In contrast, once the cell overcomes the energy barrier, a larger stretch modulus will help drive the daughter cells to complete division to minimize their surface area. Increasing the cortical stretch modulus by overexpressing dynacortin should make the initial deformation more difficult, perhaps generating a cytokinesis defect. Softer cells such as the *dynacortin* mutants would still progress through cytokinesis. However, *dynacortin* mutants do have altered cytokinesis morphology. *Cortexillin-I* mutants complete cytokinesis relatively efficiently but also suffer from morphological defects. As the stretch modulus plays a dual role in cell shape changes, it is possible that there may be a window of acceptable viscoelasticity. The cell requires large enough viscoelasticity to maintain normal kinetic and shape control, but not so much that the contractile apparatus cannot overcome the energy barrier.

Historical perspective

Researchers have been interested in cytokinesis since the 19th century (reviewed in Rappaport, 1996). Certainly, it has been long appreciated that cytokinesis is a mechanical process that involves force generation and mechanical changes of the equatorial and global cortices. Biophysical

studies of large echinoderm eggs (cells that are orders-of-magnitude larger than *Dictyostelium*) revealed that the cleavage furrow cortex became more stiff than the global cortex and that the cleavage furrow cortex generated nN-scale forces (for example, Hiramoto, 1963; Wolpert, 1966; Rappaport, 1967; Hiramoto, 1990). These previous studies are consistent with our observations in *Dictyostelium* that global and equatorial actin crosslinking specify the dimensions (D_x) of the cleavage furrow. Thus, this paper provides essential groundwork for developing a quantitative molecular and mechanical understanding of cytokinesis. Ultimately, by combining highly quantitative approaches with biochemistry and interaction genetics in a single cell type, we will dissect the complexity and robustness of cytokinesis, a process that serves as an elegant model cell shape change.

Materials and methods

Constructs and strains

Dynacortin (dynacortin aa 1–354), N173 (dynacortin aa 1–172) and C181 (dynacortin aa 173–354) were expressed using pLD1A15SN (Figure 1). We used the full-length dynacortin (pLD1A15SN:dynacortin) and C181 (pLD1A15SN:dynacortin 2B19) constructs, which were described previously (Robinson and Spudich, 2000a). pLD1A15SN:N173 was constructed using PCR with the addition of *Sal*I and *Not*I sites at the ends flanking the initiator ATG and a stop codon, respectively. CortI 2A19 was described previously (Robinson and Spudich, 2000a). GFP-N173, C181-GFP, and GFP-cortexillin-I were constructed using our GFP-tagging cassette construct and the *cortexillin-I* cDNA was derived from cortI 2A19 cDNA, as previously described (Robinson and Spudich, 2000a).

pLD1A15SN:dynhp was engineered by first subcloning into pLD1A15SN a PCR product of the full-length dynacortin cDNA in which a *Sal* I site had been introduced at the 3′ end and a *Not* I site had been introduced at the 5′ end. Then, a PCR product that included the C181 region with 5′ *Not* I and 3′ *Mlu* I sites was subcloned. The dynacortin hairpin construct reduced the expression of dynacortin to undetectable levels in wild-type and *cortI*^{1151} strains (Figure 1C). Wild-type (Ax3:orf7-3; HS1000) and *cortI*^{1151} (HS1151) cells have been described previously (Robinson and Spudich, 2000a).

For quantification of growth rates, each strain was grown in suspension culture, and cell number was measured using a hemacytometer as described (Robinson and Spudich, 2000a). For quantification of the protein amounts in each strain, a dilution series of lysates and purified protein were prepared and analyzed by Western immunoblot analysis using antidynacortin antibodies as described previously (Robinson *et al*, 2002c). Each protein was compared to known amounts of the matching purified recombinant protein. Signal from the immunoblot was generated using Amersham's ECL reagent and collected and quantified using a BioRad Versadoc imaging system.

Immunocytochemistry

To assess the localization of endogenous dynacortin, overexpressed dynacortin, N173, and C181, mid-log phase cells were fixed and stained as described previously (Robinson and Spudich, 2000a), except that the fixation buffer used was 4% paraformaldehyde, 150 mM NaCl, 0.1% Triton X-100. Indirect detection was achieved using fluorescein isothiocyanate-conjugated donkey anti-rabbit secondary antibodies (Pierce). Cells were imaged using a Zeiss Axiovert 135 microscope with a 40X (NA1.3) oil immersion objective and a 1.6X optivar. Images were collected using IPLab software package (Scanalytics) and processed using Adobe Photoshop (Adobe Systems Inc.).

Live cell imaging

To image the GFP fusion proteins, log phase cells were plated in imaging chambers. After attachment, the media were replaced with MES starvation buffer (50 mM MES pH 6.8, 2 mM $MgCl_2$ and 0.2 mM $CaCl_2$). Cells were imaged using a 40X (NA1.3) oil objective and a 1.6X optivar on a Zeiss Axiovert microscope. Images were collected using IPLab software (Scanalytics).

To image cells undergoing cytokinesis, log phase cells were plated in imaging chambers in enriched HL-5 media. Imaging was performed with the same objective and optivar setting as for GFP-fusion proteins. Rather than the suggested phase ring, the phase 2 ring was used to give higher contrast while avoiding the 'phase halo' that comes from the unmatched refractive index of the media. The phase halo subsequently obscures some of the fine details of the furrow and bridge as it proceeds. Images were collected every 2 s. Green, UV, and IR filters were added to eliminate phototoxicity and heating from the Köhler illumination.

Laser-tracking microrheology

To determine the viscoelasticity of cell cortices, we used laser-tracking microrheology (LTM). The LTM system has been described in detail elsewhere (Mason *et al*, 1997; McGrath *et al*, 2000; Yamada *et al*, 2000). Briefly, the mechanical properties of a material are inferred from the Brownian motions of embedded probe particles. Motions of probe particles are detected using a low-powered laser (0.13 mW, $\lambda = 670$ nm) focused on the particle and a quadrant photodiode detector to detect off-axis motions of the forward-scattered light. To develop LTM for the study of cortical mechanics of *D. discoideum* cells, we monitored the motion of beads attached to the extracellular surface of the cell cortex. *D. discoideum* mutant strains were removed from the incubator during log-phase growth when 40–80% confluent, washed twice with 1 ml of 1 × PB (20 mM Na_2HPO_4, 20 mM NaH_2PO_4, pH 6.9), and resuspended at a final concentration of 1×10^6 cells/ml. About 20 µl of washed cells were transferred to double-stick tape-glass slide flow cell, and 0.70-µm-diameter carboxylated polystyrene beads (Bangs Laboratories, Inc.) were then added. For latrunculin B-treated cells, 7.5-µM latrunculin B was added to the cells along with the polystyrene beads.

As particles are not fully embedded in a large cytoskeletal network, the original equations for extracting moduli from particle motions are no longer appropriate. Although models exist for extracting moduli of motions of spheres half-embedded in sheet-like materials (Bausch *et al*, 1998), key parameters cannot be measured in our system. Rather than making *ad hoc* geometric assumptions, we chose to measure the viscoelasticity, $\mu^*(\omega)$, as a combination of a phenomenological spring ($\mathrm{Re}(\mu^*) = \mu'$) and dashpot ($\mathrm{Im}(\mu^*) = \mu''$), with both elements having frequency-dependent values. Hence, $\mu^*(\omega) = [2\,k_B T / \langle \Delta R^2(\tau) \rangle]_{\omega = 1/\tau}$, which is equivalent to $\mu^*(\omega) = 6\pi a G^*(\omega)$ where a is the particle radius, thus removing any geometry-dependent assumptions. The phase angle, $\delta(\delta = \arctan(\mu''/\mu'))$, relates the liquid- to solid-like properties of the material. In all LTM statistics, each tracking event represents one bead on a unique cell (i.e. average of 11 sequential 1 s acquisitions).

Supplementary data

Supplementary data are available at *The EMBO Journal* Online.

Acknowledgements

We thank Mark Landree, Greg Huyer, Pablo Iglesias, Lynn Cooley (Yale University), Pere Puigserver, anonymous referees, and members of the Robinson lab for helpful comments on the manuscript. We thank Wendy Zhang (University of Chicago) for numerous helpful discussions. We thank the Burroughs-Wellcome Fund (DNR) and the NIH (R01 #GM066817 to DNR and R01 #GM59285 to SCK) for their support.

References

Bausch AR, Ziemann F, Boulbitch AA, Jacobson K, Sackmann E (1998) Local measurements of viscoelastic parameters of adherent cell surfaces by magnetic bead microrheometry. *Biophys J* **75:** 2038–2049

Dai J, Ting-Beall HP, Hockmuth RM, Sheetz MP, Titus MA (1999) Myosin I contributes to the generation of resting cortical tension. *Biophys J* **77:** 1168–1176

DeLozanne A, Spudich JA (1987) Disruption of the *Dictyostelium* myosin heavy chain gene by homologous recombination. *Science* **236:** 1086–1091

Devore JJ, Conrad GW, Rappaport R (1989) A model for astral stimulation of cytokinesis in animal cells. *J Cell Biol* **109:** 2225–2232

Entov VM, Hinch EJ (1997) Effect of a spectrum of relaxation times on the capillary thinning of a filament of elastic liquid. *J Non-Newtonian Fluid Mech* **72:** 31–53

Faix J, Steinmetz M, Boves H, Kammerer RA, Lottspeich F, Mintert U, Murphy J, Stock A, Aebi U, Gerisch G (1996) Cortexillins, major determinants of cell shape and size, are actin-bundling proteins with a parallel coiled-coil tail. *Cell* **86:** 631–642

Faix J, Weber I, Mintert U, Köhler J, Lottspeich F, Marriott G (2001) Recruitment of cortexillin into the cleavage furrow is controlled by Rac1 and IQGAP-related proteins. *EMBO J* **20:** 3705–3715

Feneberg W, Westphal M, Sackmann E (2001) Dictyostelium cells' cytoplasm as an active viscoplastic body. *Eur Biophys J* **30:** 284–294

Gerald N, Dai J, Ting-Beall HP, DeLozanne A (1998) A role for Dictyostelium RacE in cortical tension and cleavage furrow progression. *J Cell Biol* **141:** 483–492

Gittes F, Schnurr B, Olmsted PD, MacKintosh FC, Schmidt CF (1997) Microscopic viscoelasticity: shear moduli of soft materials determined from thermal fluctuations. *Phys Rev Lett* **79:** 3286–3289

Hiramoto Y (1963) Mechanical properties of sea urchin eggs II. Changes in mechanical properties from fertilization to cleavage. *Exp Cell Res* **32:** 76–88

Hiramoto Y (1990) Mechanical properties of the cortex before and during cleavage. *Ann NY Acad Sci* **582:** 22–30

Knecht DA, Loomis WF (1987) Antisense RNA inactivation of myosin heavy chain gene expression in *Dictyostelium discoideum*. *Science* **236:** 1081–1086

Mason TG, Ganesan K, van Zanten JH, Wirtz D, Kuo SC (1997) Particle tracking microrheology of complex fluids. *Phys Rev Lett* **79:** 3282–3285

Matzke R, Jacobson K, Radmacher M (2001) Direct, high-resolution measurement of furrow stiffening during division of adherent cells. *Nat Cell Biol* **3:** 607–610

McGrath JL, Hartwig JH, Kuo SC (2000) The mechanics of F-actin microenvironments depend on the chemistry of probing surfaces. *Biophys J* **79:** 3258–3266

O'Connell CB, Warner AK, Wang Y (2001) Distinct roles of the equatorial and polar cortices in the cleavage of adherent cells. *Curr Biol* **11:** 702–707

Rappaport R (1967) Cell division: direct measurement of maximum tension exerted by furrow of echinoderm eggs. *Science* **156:** 1241–1243

Rappaport R (1996) *Cytokinesis in Animal Cells*. Cambridge: Cambridge University Press

Robinson DN (2001) Cell division: Biochemically controlled mechanics. *Curr Biol* **11:** R737–R740

Robinson DN, Cavet G, Warrick HM, Spudich JA (2002a) Quantitation of the distribution and flux of myosin-II during cytokinesis. *BMC Cell Biol* **3:** 4

Robinson DN, Girard KD, Octtaviani E, Reichl EM (2002b) Dictyostelium cytokinesis: from molecules to mechanics. *J Musc Res Cell Motil* **23:** 719–727

Robinson DN, Ocon SS, Rock RS, Spudich JA (2002c) Dynacortin is a novel actin bundling protein that localizes to dynamic actin structures. *J Biol Chem* **277:** 9088–9095

Robinson DN, Spudich JA (2000a) Dynacortin, a genetic link between equatorial contractility and global shape control discovered by library complementation of a *Dictyostelium discoideum* cytokinesis mutant. *J Cell Biol* **150:** 823–838

Robinson DN, Spudich JA (2000b) Towards a molecular understanding of cytokinesis. *Trends Cell Biol* **10:** 228–237

Sato M, Schwarz WH, Pollard TD (1987) Dependence of the mechanical properties of actin/α-actinin gels on deformation rate. *Nature* **325:** 828–830

Simson R, Wallraff E, Faix J, Niewöhner J, Gerisch G, Sackmann E (1998) Membrane bending modulus and adhesion energy of wild-type and mutant cells of *Dictyostelium* lacking talin or cortexillins. *Biophys J* **74:** 514–522

Wachsstock DH, Schwarz WH, Pollard TD (1993) Affinity of α-actinin determines the structure and mechanical properties of actin filament gels. *Biophys J* **65:** 205–214

Wachsstock DH, Schwarz WH, Pollard TD (1994) Cross-linker dynamics determine the mechanical properties of actin gels. *Biophys J* **66:** 801–809

Weber I, Gerisch G, Heizer C, Murphy J, Badelt K, Stock A, Schwartz J-M, Faix J (1999) Cytokinesis mediated through the recruitment of cortexillins into the cleavage furrow. *EMBO J* **18:** 586–594

Weber I, Neujahr R, Du A, Köhler J, Faix J, Gerisch G (2000) Two-step positioning of a cleavage furrow by cortexillin and myosin II. *Curr Biol* **10:** 501–506

White JG, Borisy GG (1983) On the mechanisms of cytokinesis in animal cells. *J Theor Biol* **101:** 289–316

Wolpert L (1966) The mechanical properties of the membrane of the sea urchin egg during cleavage. *Exp Cell Res* **41:** 385–396

Xu J, Wirtz D, Pollard TD (1998) Dynamic cross-linking by α-actinin determines the mechanical properties of actin filament networks. *J Biol Chem* **273:** 9570–9576

Yamada S, Wirtz D, Kuo SC (2000) Mechanics of living cells measured by laser tracking microrheology. *Biophys J* **78:** 1736–1747

Zhang WW, Lister JR (1999) Similarity solutions for capillary pinch-off in fluids of differing viscosity. *Phys Rev Lett* **83:** 1151–1154

Supplementary Material

Supplementary Results

Hydrodynamics of dynacortin, N173 and C181

Dynacortin is an 80 kDa dimer with a large, 6 nm Stoke's radius (Robinson et al., 2002). Thus, dynacortin appears to be nonglobular, which is consistent with its high percentage of hydrophilic amino acid residues (Bairoch et al., 1997). We used platinum rotary shadowing and electron microscopy to view dynacortin, N173 and C181. Dynacortin appeared as elongated rods (Supplementary Figure 1A, B). Dynacortin particle size was 17 nm, which reduced to 15 nm after adjustment for platinum thickness (see Supplementary Methods; Supplementary Table 1). This is in close agreement with the Stoke's diameter (12 nm) determined from size exclusion chromatography (Supplementary Table 1). We then measured the hydrodynamic radius and the length of N173 and C181 (Supplementary Figure 1B; Supplementary Table 1). The lengths of each of these proteins after correction for platinum thickness were 6.1 nm and 7.9 nm, respectively.

Since C181 caused a downshift in the Stoke's radius of endogenous dynacortin when expressed in *D. discoideum* cells (Robinson and Spudich, 2000), we hypothesized that it might provide the dimerization domain. We analyzed N173 and C181 by sedimentation equilibrium centrifugation (Supplementary Figure 1C). The monomer molecular mass (MW) of His-N173 was calculated to be 20445.25 Da and by sedimentation analysis, N173 had a molecular mass of 20717 ± 389 Da (n=25) in salt ranging from 2-300 mM NaCl. Thus, N173 remains as monomers (Supplementary Table 1). For His-C181, the calculated MW was 21771.89 Da and by sedimentation analysis, the MWapp was 41212 ± 1600 Da (n=7). Thus, C181 forms dimers, providing the basis for dimerization of full-length dynacortin.

Analysis of the actin binding and cross-linking properties of N173 and C181

We examined and compared the actin binding and cross-linking properties of full-length dynacortin, N173 and C181, using co-sedimentation. N173 and C181 bound and cross-linked actin filaments (Supplementary Figure 2A). We used high-speed (100,000xg) sedimentation to measure total binding of protein to actin and low-speed (10,000xg) sedimentation to measure the formation of larger complexes of cross-linked actin. Because it is not necessary for saturation of the bundled complex to have the same stoichiometry as saturation of total actin, we first

determined the saturation ratios of dynacortin, N173 and C181 under both conditions (Supplementary Figure 2B). Dynacortin and C181 saturated actin at a ratio of two moles of protein per mole of actin under both conditions. Since dynacortin and C181 are dimers, this indicates a ratio of one dimer per actin. In contrast, N173 saturated actin at a ratio of one monomer per actin under both conditions.

Given the saturation stoichiometries of full-length dynacortin and each of the half molecules and since at least two actin filaments are required to form a bundle, we used the binding models in Supplementary Figure 2C to evaluate our binding data. We analyzed the formation of bound complexes and cross-linked complexes by mixing protein and actin together in duplicate reactions then sedimenting the samples under high-speed and low-speed in parallel. Holding the actin constant over a variety of concentrations, we varied the protein so that we examined a wide range of protein and actin concentrations. We calculated K_{D1app} ($(1/K_1)^{1/2}$) from the high-speed samples and calculated $1/K_1K_2$ from the low-speed samples. From these two numbers, we were able to calculate K_{D2app} ($1/K_2$). In Table 2, we present data for K_{D1app} using 5-μM actin. The data for K_{D2app} is from a wide variety of actin concentrations, ranging from 1-20 μM actin. Our analysis determined that K_{D1app} is dependent on the actin concentration, rising linearly with increasing concentration. K_{D2app}, in contrast, was not actin-concentration dependent. Although a simple chemical equilibrium is expected to be concentration independent, the results, in fact, make intuitive sense. In essence, the cross-linking protein serves to inhibit itself by sequestering away the actin filaments. Since actin is a polymer, a few cross-links can quickly bury actin filaments (and hence available binding sites for additional cross-linking proteins). The apparent affinity then declines with increasing actin concentrations. Once the cross-linkers bind to the first actin, they can cross-link the second actin so that K_{D2app} is actin-concentration independent. Across all of our experiments the initial binding affinities of dynacortin and N173 for actin are indistinguishable. In contrast, C181 always showed a 2-3 fold lower affinity for initial binding. Dynacortin and C181 had similar K_{D2app} values, indicating that their ability to form bundles once bound to actin filaments is more similar. N173 had a lower affinity for cross-link formation than either of the other two. The relative abilities to bind and cross-link actin is reflected by $1/K_1K_2$ (Main text Table 2).

Analysis of the actin bundling activities of dynacortin and its domains

To verify that dynacortin, N173, and C181 are cross-linking and bundling actin, we assembled the bundles, then negatively stained and examined them by transmission electron microscopy (Supplementary Figure 3A). Dynacortin formed large parallel bundles as was anticipated from prior experiments (Robinson et al., 2002). C181 assembled the actin filaments into bundles that were morphologically indistinguishable from those formed by full-length dynacortin. N173 formed small bundles and cross-linked meshworks at similar concentrations but required much higher concentrations to form parallel bundles, though they never reach the large sizes observed for dynacortin and C181 (data not shown).

For a more quantitative view of the ability of each proteins to bundle actin, we developed a simple quantitative assay using fluorescence microscopy (Supplementary Figure 3 B, C). The assay used 1-μM rhodamine-phalloidin stabilized actin filaments and varying concentrations of dynacortin, N173, and C181. To quantitate the dynacortin, N173, and C181 concentration dependency of bundle formation, the standard deviation of the pixel intensity was calculated using unmodified digital micrographs. This parameter gave the best representation of the images. The rationale is that for images where the actin filaments are unbundled, the actin filaments fill the field, giving a relatively even field of fluorescence. As the filaments become bundled, more pixels acquire a high level of signal while a substantially larger number of pixels yield no signal. This leads to a bimodal distribution of pixel intensities, which is reflected in the standard deviation of pixel intensity. We calculated the mean of these standard deviations from six or more fields for each protein concentration. Then, plotting the standard deviation of pixel intensity versus protein concentration leads to a quantitative representation of the bundling by each protein. From this assay, the concentration of dynacortin that produced the half-maximal bundling activity was 1 μM (0.5-μM dynacortin dimer). N173 and C181 had half-maximal concentrations of around 60 μM and 15 μM (7.5-μM dimer), respectively. Thus, N173 and C181 are poorer bundlers than dynacortin, though C181 has properties that are more similar overall to the full-length dynacortin.

For an independent analysis of actin cross-linking behavior, we used falling ball viscometry to assess the concentration dependence of actin cross-linking (Supplementary Figure 3D). None of the proteins increased the apparent viscosity at extremely low concentrations

above actin-alone controls. However, only 0.5-1 μM dynacortin was required to increase the viscosity of 24-μM actin gels. By increasing the concentration of dynacortin to 2 μM, the actin became bundled, resulting in a phase separation. This is due to the concentration of the actin into bundles, producing a heterogeneous solution with regions devoid of actin bundles and low viscosity and regions where the bead was obstructed by the actin bundle mass. The data were uninformative in this regime. Significantly higher C181 dimer concentrations (15 μM) were required to increase the viscosity of the gel, though the amount of increase (2-3 fold) before phase separation was smaller than for dynacortin. 50-60 μM N173 was required to increase the viscosity of the actin gel. Intriguingly, the viscosity was increased much more (20-fold) by N173 than for either the full-length or C181 domains. Though N173 appears to be a poorer bundler, it appears to be a good cross-linker at high concentrations. Notably, the [cross-linker]-dependency determined by falling ball viscometry (which uses 24-μM filamentous actin) and the [cross-linker]-dependency from the fluorescence bundle assay (1-μM filamentous actin) were in close agreement.

In summary, dynacortin is more effective at actin cross-linking than either N173 or C181. But, each half domain is capable of binding and bundling actin filaments. The equilibrium constants indicate that both N173 and C181 cross-link with similar thermodynamics that are only somewhat lower than full-length dynacortin. However, from the cross-linking and bundling assays, an activity order is indicated in which dynacortin > C181 > N173. Since N173 and C181 bound actin with similar thermodynamics, it is possible that N173 has faster on and off rates than C181 or dynacortin, allowing it to achieve similar overall thermodynamics of actin cross-linking. These differences in actin cross-linking have implications for how each domain may influence the viscoelastic properties of the cortex.

Supplementary Materials and Methods

Constructs and Strains

Dynacortin (dynacortin a.a. 1-354), N173 (dynacortin a.a. 1-172) and C181 (dynacortin a.a. 173-354) were expressed using the pET14b (Novagen) expression plasmid (Figure 1). Constructs were generated using polymerase chain reaction and subcloned into the *Nde* I and *Bam*H I sites. The resulting plasmid encodes a 6xHis tag, followed by a thrombin cleavage site

then the complete dynacortin derivative. Stop codons were introduced at the end of the dynacortin peptide so as not to include any additional amino acid residues.

Protein expression and purification

For expression, we engineered an expression strain using BLR cells (Novagen) and the helper plasmid (pRARE), which includes the LysS and tRNAs for rare Arg, Ile, and Leu codons that is included in the Rosetta (Novagen) *Escherichia coli* cells. This plasmid was isolated from the Rosetta cells and introduced into BLR cells. We named the resulting strain BLAREs (BLR:pRARE). The advantage of this strain is that it now includes the DE3 lysogen for IPTG inducible expression of the T7 polymerase, lysozyme activity, rare tRNAs to help with the *D. discoideum* codon usage bias, and the *RecA* mutation. This combination of features increased expression 6-7-fold for full-length dynacortin as compared to what we have observed using other *E. coli* expression strains.

To begin purification, cultures were grown to an optical density of 0.6 at 600 nm. Expression was induced with 0.4 mM IPTG and cells were allowed to express for four hours. Cells were harvested by centrifugation, washed with 10 mM Tris pH 7.5, and resuspended at a density of one liter of cell culture equivalent per 30 mls of lysis buffer. Lysis buffer included 20 mM NaCl, 10 mM Hepes pH 7.1, 1 mM EDTA, and 1mM EGTA and a cocktail of protease inhibitors including the following: 0.1 mM phenylmethylsulfonyl fluoride, 150 μM 1-chloro-3-tosamido-7-amino-2-heptanone, 80 μg/ml L-1-tosylamido-2-phenylethyl chloromethyl ketone, 1 mg/ml benzamidine, 100 μg/ml Nα-*p*-tosyl-L-arginine-methyl ester, and 5 μg/ml leupeptin. Cells were lysed by freeze-thaw in liquid N_2. Lysates were clarified by centrifugation at 34,000xg for 25 minutes followed by precipitation with 0.25% polyethylenimine. The polyethylenimine precipitates were removed by centrifugation and the supernatants were fractionated by the addition of solid ammonium sulfate to 45% saturation. Full-length dynacortin, N173 and C181 each precipitate with the addition of 45% ammonium sulfate, resulting in a huge enrichment of each protein. The ammonium sulfate precipitates were solubilized in no salt A buffer (10 mM Hepes pH 7.1) and filtered through a 0.2 μm syringe filter to prepare the proteins for subsequent chromatographic steps using a BioRad Duo-Flow fast phase liquid chromatography system.

Full-length dynacortin was further purified first by separation on a Sephacryl S300 size exclusion column (Amersham) using the following buffer: 200 mM NaCl, 10 mM Hepes pH 7.1. Dynacortin eluted from this column with a K_{av} of 0.25. Fractions were pooled, diluted two-fold with no salt A and separated with a 20-column volume linear salt gradient from 28% B to 40% B where buffer B is 1 M NaCl, 10 mM Hepes pH 7.1 on a mono S HR 5/5 column (Amersham). Pure fractions were pooled, diluted in no salt A, reapplied to the mono S HR 5/5 column and eluted with 50% buffer B to concentrate the protein. The concentrated protein was dialyzed overnight to 2 mM NaCl, 10 mM Hepes pH 7.1, 1 mM NaN_3. With the BLARE cells, we typically recover around 2 mg of purified dynacortin per liter of bacterial culture.

N173 was purified by separation on a homemade 12-ml SP-sepharose Fast Flow (Amersham) column. The protein was eluted with a 10-column volume 20% B to 40% B gradient. The purified N173 was pooled, diluted two-fold in no salt A and concentrated on a monoS HR 5/5 (Amersham) column similar to full-length dynacortin. The protein was dialyzed into the same dialysis buffer. 1-2 mg of purified N173 per liter of bacterial culture were recovered from this protocol.

C181 was purified by separation on the same 12-ml SP sepharose but eluting with a 0-40% B salt gradient. The protein was further purified and concentrated on a mono S HR 5/5 column using a 20%-45% B salt gradient. We recovered 25 mg of purified C181 per liter of cell culture.

Actin was purified from chicken skeletal muscle using the methods of Pardee and Spudich (Pardee and Spudich, 1982). G-actin was further purified using an S300 Sephacryl column equilibrated in G-actin column buffer (10 mM Tris pH 7.5, 0.3 mM $CaCl_2$, 0.1 mM EDTA, 0.7 mM ATP, 0.02% NaN_3).

Rotary shadowing electron microscopy

Dynacortin, N173 and C181 particles were diluted in buffer at 50-300 μg/ml. 50 μl of sample was further diluted with spectroscopy grade glycerol at a 50% final concentration and loaded into a nebulizer. Samples were sprayed onto freshly cleaved mica squares with a Dust-off (Falcon) air can and loaded onto a Denton DV-502A metal evaporator. Samples were rotary shadowed (1 rpm) at $4x10^{-7}$ torr with 3.7 mg of platinum (Pella). The replicas were then supported with 6 nm of evaporated carbon then floated off on a drop of distilled water. Replicas

were picked up with glow discharged 400 mesh copper grids and blot dried with #1 filter paper (Whatman). All grids were viewed and photographed on a Phillips CM-120 TEM, operating at 80 kV. The metal thickness was estimated using the following equation: $wt_{Pt} = (4\pi 2dt\rho(10^{-5}))/(\sin s)$ where wt_{Pt} is the weight of platinum that was ionized, d is the distance from the point source (7 cm in our experiments), t is the thickness in Å, ρ is the bulk density of Pt (21.45 g/cm^3), and s is the shadowing angle 8°. The average thickness, t, was calculated to be 1.25± 0.046 nm from n=5 experiments. 2t (2.5) nm was substracted from the mean particle size to get a more accurate estimate of protein size.

Sizing by size-exclusion chromatography

To measure the hydrodynamic radius of dynacortin, N173 and C181, the proteins were separated on a calibrated high resolution S200 10/30 HR size exclusion column (Amersham) equilibrated in 200 mM NaCl, 10 mM Hepes pH 7.1. The column was calibrated with blue dextran (2000 kDa, $K_{av} = 0$) to mark the void volume, thyroglobulin (669 kDa, Stoke's radius 8.5 nm, $K_{av} = 0.12$), ferritin (440 kDa, Stoke's radius 6.1 nm, $K_{av} = 0.27$), catalase (223 kDa, Stoke's radius 5.2 nm, $K_{av} = 0.39$), bovine serum albumin (67 kDa, Stokes radius 3.5 nm, $K_{av} = 0.47$), cytochrome c (12.4 kDa, Stoke's radius 1.7 nm, $K_{av} = 0.76$), and vitamin B12 (1.3 kDa, $K_{av} = 0.96$). The total volume ($K_{av} = 1.0$) was marked by the conductance change caused by the difference in salt concentration from input protein and the running buffer. From these standards, the K_{av} for each was plotted against their respective Stoke's radius, the resulting points were fit to a linear equation. The Stoke's radii of dynacortin, N173, and C181 were calculated from each protein's K_{av}.

Molecular weight determination by analytical ultracentrifugation

To determine the stoichiometry of the His-tagged N173 and C181, the protein was subjected to equilibrium sedimentation analysis using a Beckman Optima XL-I analytical ultracentrifuge (Beckman Instruments). We used the calculated mass from the primary sequence to determine the monomer molecular weights. We also examined each protein by matrix-assisted laser desorption ionization-time of flight mass spectroscopy (MALDI-TOF) using an Applied Biosystems Voyager DE-STR MALDI-TOF to confirm the calculated masses (Johns Hopkins School of Medicine Mass Spec. facility). The partial specific volumes for His-N173

and His-C181 were calculated to be 0.7056 ml/g and 0.7259 ml/g, respectively. The solvent density was calculated for different salt concentrations by summing the incremental density contributions of the constituents. All calculations including temperature corrections were made by Laue's methods (Laue et al., 1992). C181 was measured at 300 mM NaCl. N173 was measured using solvents containing 2 mM, 25 mM, 50 mM, 75 mM, 150 mM or 300 mM NaCl, or 0.5xF-buffer or 1xF-buffer (10xF-buffer: 500 mM KCl, 10 mM $MgCl_2$, 10 mM EGTA, 2 mM ATP, 10 mM DTT, 100 mM imidazole, pH 7). The NaCl buffers contained 10 mM Hepes, pH 7.1. Initial protein concentrations ranged from 7.5 to 40 μM protein. Protein concentration was monitored by absorption at 280 nm. Initial concentration readings were taken at 3000 rpm. The samples were centrifuged at 16000, 17000, and 18000 rpm for at least 26 hours, then scans were taken every 2 hours until the sample reached equilibrium. Absorption curves were integrated after equilibrium and compared to the integrated absorption of the initial scan at 3000 rpm. The fractional amount of protein in the cell after reaching equilibrium compared to the initial sample was 0.99 ± 0.02 (n= 35; mean ± SEM) for N173 and 0.99 ± 0.02 (n=15; mean ± SEM) for C181, verifying that the measured molecular weight accurately reflects the population of protein and that there is no significant loss due to precipitation during the centrifugation. The average MWapp was determined by fitting multiple data files to a single ideal species model. All fits were performed using the Microcal Origin software (Beckman Instruments).

Analysis of actin interactions

***In vitro* cosedimentation:** G-actin was allowed to polymerize at high concentrations for 30 min at 22ºC by the addition of 10x Mg-exchange buffer (3 mM EGTA, 2 mM $MgCl_2$, 10 mM Tris, pH 7.5) followed by 10x-polymerization buffer (500 mM KCl, 10 mM $MgCl_2$, 10 mM EGTA, 2 mM ATP, 10 mM DTT, 100 mM imidazole, pH 7) to a final concentration of 1x for each buffer. Both actin and His-dynacortin were centrifuged to remove any aggregates before the assays were performed. Actin and His-dynacortin, N173 or C181 were mixed to appropriate concentrations and the dialysis buffer matched to each protein was added to normalize the volume of buffer from the dynacortin-derived protein. The reactions contained a final concentration of 0.5x or 1x polymerization buffer. Samples were incubated for 1 hr at 22ºC and sedimented at 100,000xg (total actin binding) in a TL100 ultracentrifuge for 25 min or at 10,000xg (actin bundling) in a microfuge for 25 min. Each reaction was prepared in duplicate so that one sample was

sedimented to analyze total actin binding and one sample was sedimented to analyze bundle formation. Supernatant and pellet fractions were collected, resuspended to a final concentration of 1x Laemmli's sample buffer and equivalent amounts were loaded on 15% SDS-PAGE gels. Gels were stained in Coomassie Blue stain and destained in 10% acetic acid. Proteins were quantified using an AlphaImager densitometer (Alpha Innotech Corp.). The linear ranges for dynacortin, N173, C181 and actin concentrations were determined so only appropriate amounts at each concentration were loaded on the gel for accurate quantification.

Electron microscopy: Various concentrations of His-dynacortin, N173, and C181 and 1-μM F-actin were mixed in 1x polymerization buffer and incubated for approximately 1 hr. Carbon coated copper grids were incubated with the protein mixture for 2 min. The grids were washed one time in filtered water and then grids were incubated in two changes of 1% uranyl acetate with 0.04% tylose for one min. each. Grids were dried by blotting on #1 filter paper (Whatman). All grids were imaged using a Phillips CM-120 TEM, operating at 80 kV.

Fluorescence microscopy: To examine the formation of actin bundles by light microscopy, actin filaments were labeled at a 1:1 mole ratio with tetramethyl rhodamine-labeled phalloidin (Molecular Probes). Varying concentrations of dynacortin, N173, and C181 were mixed with 1-μM labeled actin filaments and viewed on a Zeiss Axiovert fluorescence microscope using a 40X oil (NA=1.4) objective and a 1X optivar. Images were acquired using IP Lab (Scanalytics). Multiple images were acquired for each sample. All images were acquired using identical exposure times, filters, etc. From digital images of the samples, the standard deviation of the fluorescence intensity was determined for the population of pixels from the micrograph using Adobe Photoshop (Adobe Systems, Inc.).

Falling Ball Viscometry: For falling-ball viscometry (MacLean-Fletcher and Pollard, 1980), we mixed 1 mg/ml G-actin with varying concentrations of dynacortin, N173 or C181. 10x-polymerization buffer was added to a final concentration of 1x. The samples were immediately drawn into microcapillary pipets (VWR), capped, and incubated at 25°C for 3-4 hr. The viscosity, η, is inversely proportional to the velocity of the ball and proportional to constant $c = mg/(\sin\Theta * 6\pi r)$, where m is the mass of the ball, g is gravity, r is the ball radius and Θ is the angle of the tube (50° in our experiments). We used water (η = 1 mPa•s) and glycerol (η = 1408 mPa•s) to determine c for our set up. c was determined each day using standards. The velocity of a 0.7-mm steel ball was measured as it fell through the standards, uncross-linked actin gels, or

cross-linked actin gels. The viscosity, η, of actin gels without cross-linker was measured each day so that the viscosity of the cross-linked gels could be measured relative to actin-alone controls. This allowed for temperature and prep-to-prep variations to be accounted for though these variations amounted to at most 20-30% percent differences in c.

Supplementary References

Bairoch, A., Bucher, P. and Hofmann, K. (1997) The PROSITE database, its status in 1997. *Nucl. Acids Res.*, **25**, 217-221.

Laue, T.M., Shah, B.D., Ridgeway, T.M. and Pelletier, S.L. (1992) Computer-aided interpretation of analytical sedimentation data for proteins. In Harding, S., Rowe, A. and Horton, J.C. (eds.), *Analytical Ultracentrifugation in Biochemistry and Polymer Science*. Royal Society of Chemistry, Cambridge.

MacLean-Fletcher, S.D. and Pollard, T.D. (1980) Viscometric analysis of the gelation of Acanthamoeba extracts and purification of two gelation factors. *J. Cell Biol.*, **85**, 414-428.

Pardee, J.D. and Spudich, J.A. (1982) Chapter 18: Purification of muscle actin. *Methods Cell Biol.*, **24**, 271-289.

Robinson, D.N., Ocon, S.S., Rock, R.S. and Spudich, J.A. (2002) Dynacortin is a novel actin bundling protein that localizes to dynamic actin structures. *J. Biol. Chem.*, **277**, 9088-9095.

Robinson, D.N. and Spudich, J.A. (2000) Dynacortin, a genetic link between equatorial contractility and global shape control discovered by library complementation of a Dictyostelium discoideum cytokinesis mutant. *J. Cell Biol.*, **150**, 823-838.

Supplementary Figure Legends

Supplementary Figure 1. Dynacortin forms 15 nm rods. A. The images are a gallery of transmission electron micrographs of platinum rotary shadowed dynacortin particle replicas. The scale bar is 20 nm and applies to all images. B. Histograms representing the size distribution of metal shadowed particles of dynacortin, N173 and C181. The means, standard errors and n values are included. The means reported here are the actual sizes of the particles before the correction for the thickness of the metal layer, which is listed in Table 1. C. Sedimentation equilibrium analytical ultracentrifugation of N173 and C181. These graphs are example absorbance traces after the protein reached equilibrium. The fits are evolved from a model of a single ideal species. The residuals from the fits are presented.

Supplementary Figure 2. N173 and C181 bind to actin filaments *in vitro*. A. Using high speed co-sedimentation, unbound (supernatant, S) and bound (pellet, P) fractions were separated and then analyzed by denaturing polyacrylamide gel electrophoresis. The respective concentration of each protein used in each reaction is indicated. The salt conditions were 0.5x polymerization buffer. Over 85% of the N173 and C181 were ultimately pelleted at the highest actin concentrations. B. Dynacortin, N173, and C181 saturably bind actin filaments under high-speed and low-speed conditions. 1-μM F-actin and 0.5x polymerization buffer were used for these experiments. All concentrations used in these experiments were for monomeric protein. Therefore, dynacortin and C181 saturated at approximately 2 moles of monomer (1 mole of dimer) per mole of actin. N173 saturated at one mole of monomer per mole of actin. C. Binding models for dynacortin, N173 and C181 were evolved by combining the hydrodynamic properties ascertained by analytical ultracentrifugation with the saturation stoichiometries determined from the co-sedimentation experiments. These models were used to assess the apparent affinities for each step of actin cross-linking. A= actin.

Supplementary Figure 3. Dynacortin is the best actin cross-linker whereas C181 and N173 require progressively higher concentrations for actin cross-linking, respectively. A. Transmission electron microscopy of actin filaments ± dynacortin, N173 and C181. The actin bundles were assembled from 2 μM-filamentous actin in 1x polymerization buffer in each case. Scale bar (200 nm) for the actin alone panel applies to all images. B. Dynacortin bundles actin

into large arrays in a concentration dependent manner. 1-μM filamentous actin is labeled with rhodamine phalloidin for visualization. The concentrations are for monomeric dynacortin. Dimeric concentrations then are half of the value indicated. Scale bar (10 μm) applies to all panels. C. Dynacortin and its C181 and N173 domains have a cross-linking activity order of Dynacortin>C181>N173. The plots show how the mean standard deviation varies as a function of cross-linker concentration. Each point is the average of typically 6 or more micrographs per protein concentration. D. Relative actin cross-linking activities were measured using falling ball viscometry. Actin-alone controls were measured each day and all viscosities were normalized to the actin-alone controls for a given day. The amounts of cross-linker required to increase the apparent viscosity of 1 mg/ml actin was similar to the amounts required to increase the amount of bundling in the fluorescence assay in B and C. For dynacortin, the actin was organized into extended bundles. This results in a phase shift, which produces a mixture of dense actin bundles and actin free buffer. The beads showed a variety of high and low velocities due to drag from the bundles or low viscosity from the actin depleted domains of the capillary tube. Ordinarily, one would not expect drag from actin bundles since they are typically much smaller than the scale of the ball. However, dynacortin organizes actin filaments into bundles that can reach diameters of 1-μm and extended networks that are on the scale of the 0.7 mm ball (Robinson et al., 2002). In fact, the large networks of actin bundles are visible by eye at the higher concentrations of dynacortin. The data from these concentration ranges are indicated as gray circles to reflect the observations but to indicate that these data points are not useful for quantitative comparison.

Supplementary Table 1. Summary of the hydrodynamic properties of dynacortin, N173, and C181

Protein	Length, Pt. Shadowing (nm)	Stoke's Diameter (nm)	Stoichiometry
Dynacortin	15	12	2
N173	6.1	7.2	1
C181	7.9	8.5	2

Supplementary Table 2. P-Values from One-Tailed Student's T-Tests for |μ*| at 10 rad/sec and 100 rad/sec

10 rad/sec

	cortl^{1151}:pLD1	wt:N173	cortl^{1151}:N173	wt:C181	cortl^{1151}:C181	wt:dyn	cortl^{1151}:dyn	cortl^{1151}:cort	wt:pLD1w/lat
wt:pLD1	0.016	0.251	0.022	0.385	0.313	0.030	0.076	0.120	<0.0001
cortl^{1151}:pLD1		0.003	0.390	0.024	0.018	0.001	0.002	0.004	<0.0001
wt:N173			0.003	0.421	0.493	0.085	0.157	0.226	<0.0001
cortl^{1151}:N173				0.033	0.025	0.0002	0.003	0.005	<0.0001
wt:C181					0.432	0.107	0.158	0.216	<0.0001
cortl^{1151}:C181						0.156	0.207	0.272	<0.0001
wt:dyn							0.476	0.385	<0.0001
cortl^{1151}:dyn								0.420	<0.0001
cortl^{1151}:cort									<0.0001

100 rad/sec

	cortl^{1151}:pLD1	wt:N173	cortl^{1151}:N173	wt:C181	cortl^{1151}:C181	wt:dyn	cortl^{1151}:dyn	cortl^{1151}:cort	wt:pLD1w/lat
wt:pLD1	0.050	0.055	0.469	0.100	0.144	0.045	0.020	0.163	<0.0001
cortl^{1151}:pLD1		0.002	0.090	0.010	0.016	0.002	0.001	0.015	<0.0001
wt:N173			0.140	0.430	0.482	0.400	0.158	0.396	<0.0001
cortl^{1151}:N173				0.155	0.203	0.111	0.045	0.235	<0.0001
wt:C181					0.428	0.488	0.243	0.359	<0.0001
cortl^{1151}:C181						0.405	0.191	0.433	<0.0001
wt:dyn							0.222	0.321	<0.0001
cortl^{1151}:dyn								0.138	<0.0001
cortl^{1151}:cort									<0.0001

White Boxes: P-values ≤ 0.05

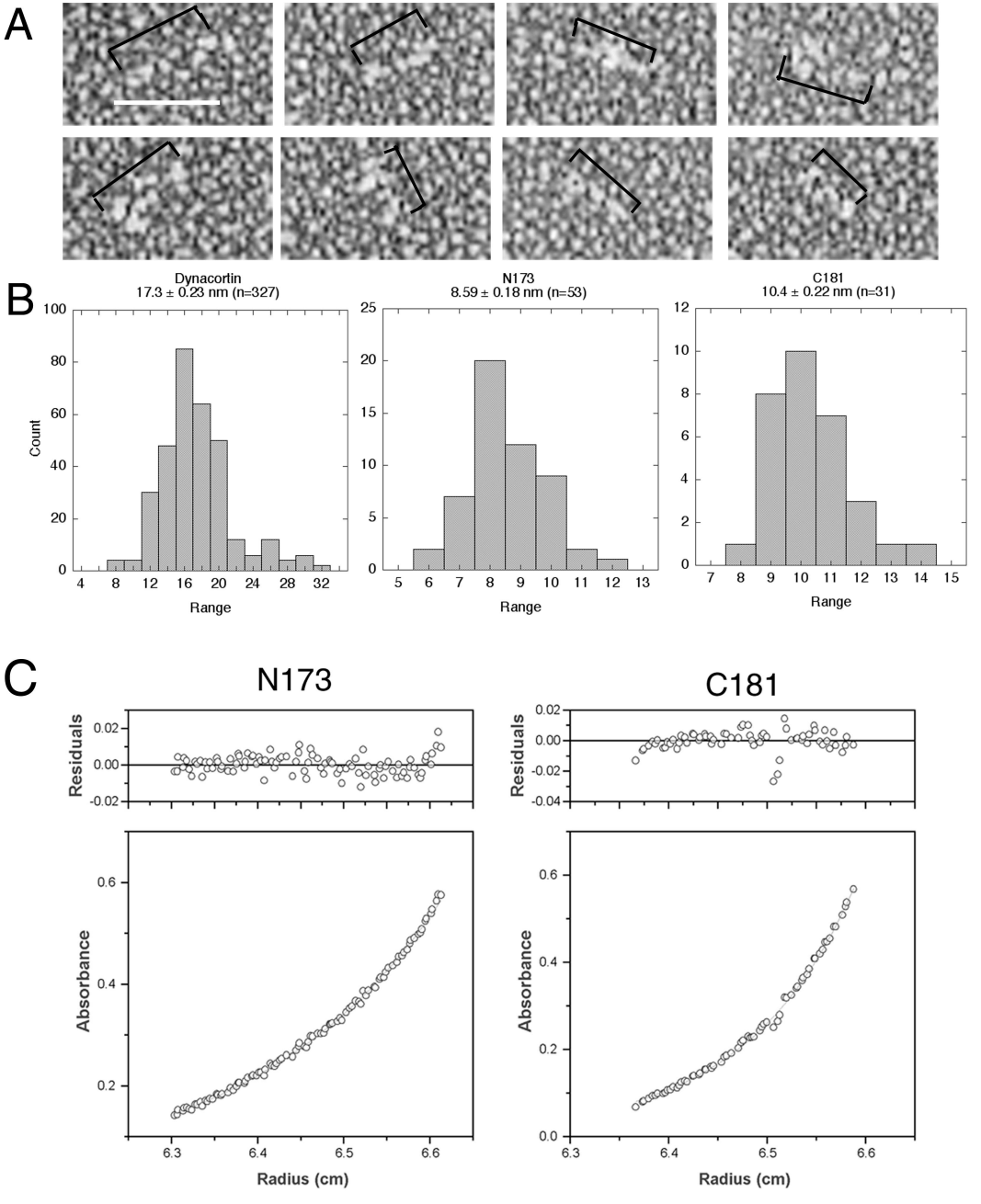

Supplementary Figure 1

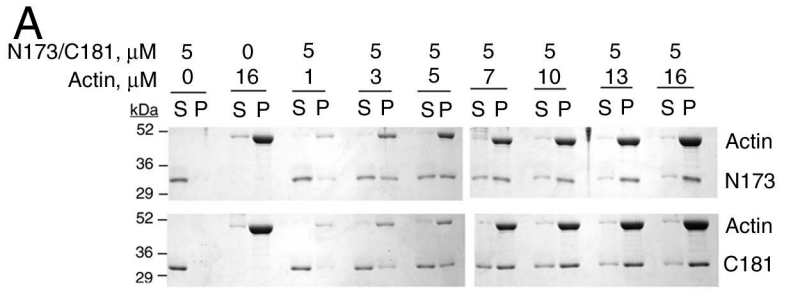

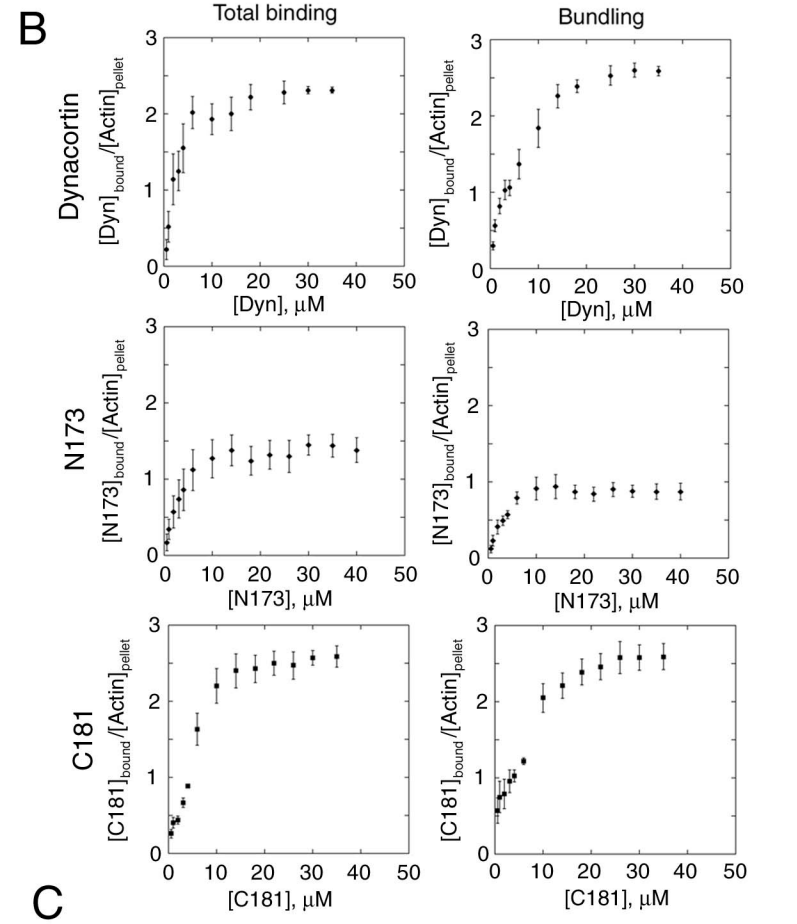

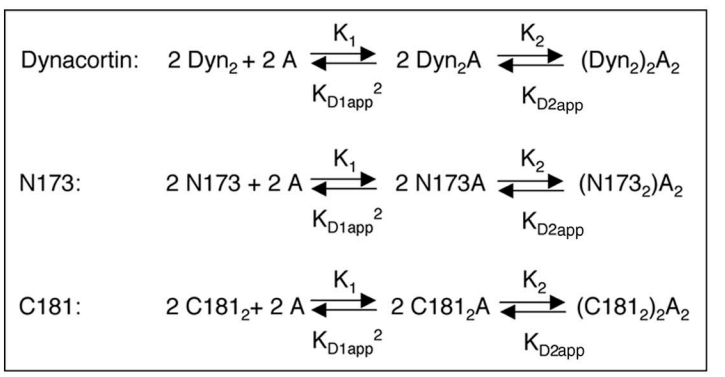

Supplementary Figure 2

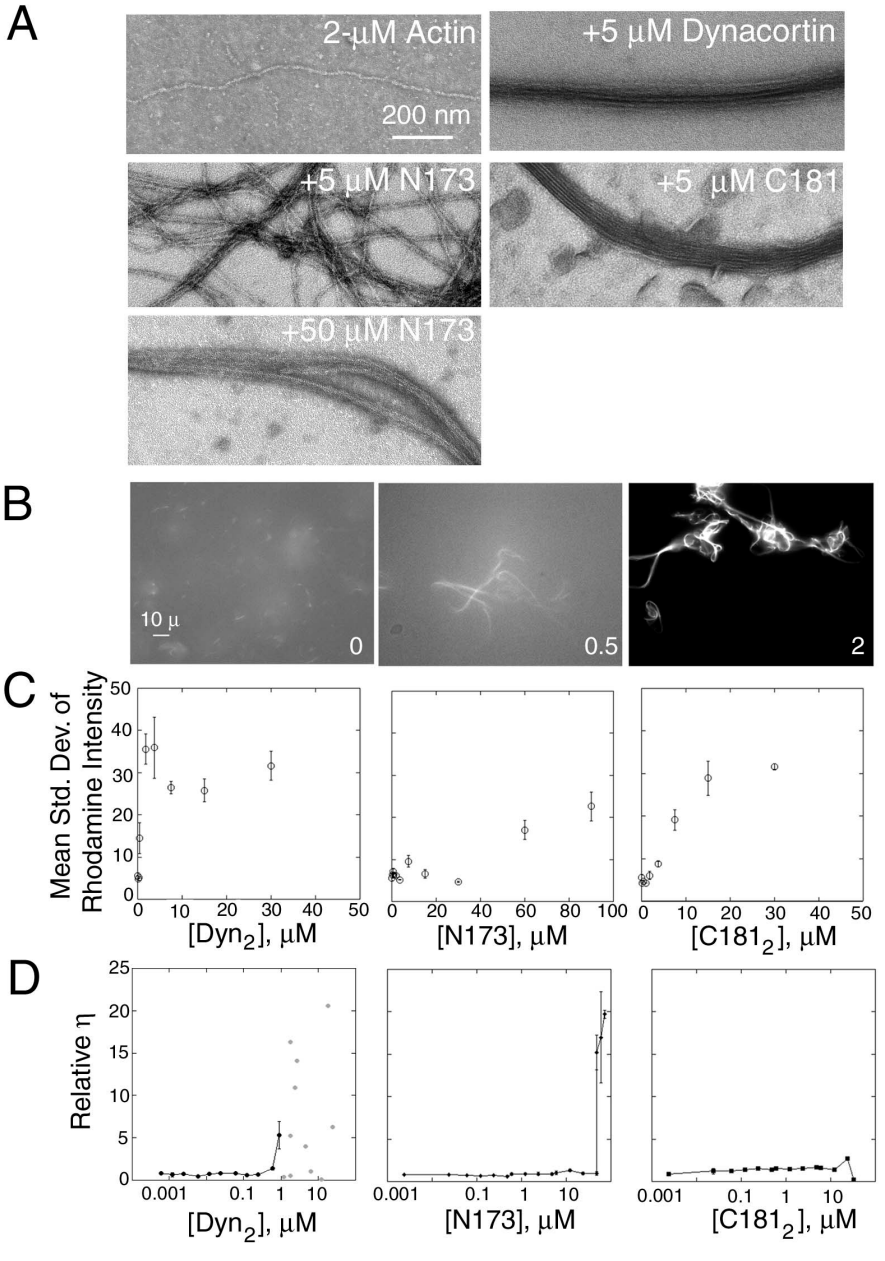

Supplementary Figure 3